

A numerical fit of analytical to simulated density profiles in dark matter haloes

R. Caimmi, C. Marmo, T. Valentinuzzi*

November 21, 2018

Abstract

Analytical and geometrical properties of generalized power-law (GPL) density profiles are investigated in detail. In particular, a one-to-one correspondence is found between mathematical parameters (a scaling radius, r_0 , a scaling density, ρ_0 , and three exponents, α , β , γ), and geometrical parameters (the coordinates of the intersection of the asymptotes, x_C , y_C , and three vertical intercepts, b , b_β , b_γ , related to the curve and the asymptotes, respectively): $(r_0, \rho_0, \alpha, \beta, \gamma) \leftrightarrow (x_C, y_C, b, b_\beta, b_\gamma)$. Then GPL density profiles are compared with simulated dark haloes (SDH) density profiles, and nonlinear least-absolute values and least-squares fits involving the above mentioned five parameters (RFSM5 method) are prescribed. More specifically, the sum of absolute values or squares of absolute logarithmic residuals, $R_i = \log \rho_{SDH}(r_i) - \log \rho_{GPL}(r_i)$, is evaluated on 10^5 points making a 5-dimension hypergrid, through a few iterations. The size is progressively reduced around a fiducial minimum, and superpositions on nodes of earlier hypergrids are avoided. An application is made to a sample of 17 SDHs on the scale of cluster of galaxies, within

*Astronomy Department, Padua Univ., Vicolo Osservatorio 2, I-35122 Padova, Italy
email: caimmi@pd.astro.it

a flat Λ CDM cosmological model (Rasia et al. 2004). In dealing with the mean SDH density profile, a virial radius, r_{vir} , averaged over the whole sample, is assigned, which allows the calculation of the remaining parameters. Using a RFSM5 method provides a better fit with respect to other methods. The geometrical parameters, averaged over the whole sample of best fitting GPL density profiles, yield $(\alpha, \beta, \gamma) \approx (0.6, 3.1, 1.0)$, to be compared with $(\alpha, \beta, \gamma) = (1, 3, 1)$, i.e. the NFW density profile (Navarro et al. 1995, 1996, 1997); $(\alpha, \beta, \gamma) = (1.5, 3, 1.5)$ (Moore et al. 1998, 1999); $(\alpha, \beta, \gamma) = (1, 2.5, 1)$ (Rasia et al. 2004); and, in addition, $\gamma \approx 1.5$ (Hiotelis 2003), deduced from the application of a RFSM5 method, but using a different definition of scaled radius, or concentration; and $\gamma \approx 1.2$ -1.3 deduced from more recent high-resolution simulations (Diemand et al. 2004; Reed et al. 2005). No evident correlation is found between SDH dynamical state (relaxed or merging) and asymptotic inner slope of the fitting logarithmic density profile or (for SDH comparable virial masses) scaled radius. Mean values and standard deviations of some parameters are calculated, and in particular the decimal logarithm of the scaled radius, ξ_{vir} , reads $\langle \log \xi_{\text{vir}} \rangle = 0.74$ and $\sigma_{s \log \xi_{\text{vir}}} = 0.15$ -0.17, consistent with previous results related to NFW density profiles. It provides additional support to the idea, that NFW density profiles may be considered as a convenient way to parametrize SDH density profiles, without implying that it necessarily produces the best possible fit (Bullock et al. 2001). A certain degree of degeneracy is found in fitting GPL to SDH density profiles. If it is intrinsic to the RFSM5 method or it could be reduced by the next generation of high-resolution simulations, still remains an open question.

keywords - cosmology: theory - dark matter - galaxies: clusters - galaxies: haloes.

1 Introduction

Recent observations of anisotropies in the cosmic microwave background put severe constraints on the cosmological parameters, by comparison with the predictions of current theories of structure formation and the evolution of the Universe. The addition of information from large-scale structure surveys, Hubble parameter determinations, and Type Ia supernova results, yields evidence for a flat ($\Omega_m + \Omega_\Lambda \approx 1$), low-density ($\Omega_m \approx 0.3$; $\Omega_\Lambda \approx 0.7$) universe, a

Zeldovich power-law index of primordial fluctuations ($n_s \approx 1$), a (non baryonic) dark matter density ($\Omega_d h^2 \approx 0.16$) dominant over baryon matter density ($\Omega_b h^2 \approx 0.023$), a Hubble parameter (normalized to $100 \text{ km s}^{-1} \text{ Mpc}^{-1}$) between one half and unity ($h \approx 0.69$), and a cosmological age between ten and fifteen billion years ($T \approx 13.7 \text{ Gyr}$), which make the main information (Sievers et al. 2003). The above mentioned values are consistent with the results deduced by different investigations (e.g., Rubiño-Martin et al. 2003; Spergel et al. 2003; Fukugita & Peebles 2004).

The related (Λ CDM) cosmological model (e.g., Diemand et al. 2004; Reed et al. 2005) is consistent with a bottom-up picture (hierarchical clustering) of dark matter haloes, where smaller systems formed first from initial density perturbations and then merged with each other to become larger systems, or were tidally disrupted and accreted from previously formed larger systems. Most naturally, the density profiles of haloes are expected to be a two-parameters family. This is why, assuming that halo formation may be approximated to an acceptable extent by spherical collapse, each protohalo perturbation is characterized by two independent parameters e.g., mass and radius (or overdensity), at some fiducial cosmological time.

A successful two-parameter functional form for the halo profile, where a scaled density depends on a scaled radius, has been proposed by Navarro et al. (1995, 1996, 1997, the last quoted hereafter as NFW). They also argued that the density profile is universal, in the sense that its shape does not appreciably change (over two decades in radius) for different halo masses (spanning about four orders of magnitude), initial density fluctuation spectra, or cosmological parameters. Many studies on the NFW “universal density profile”, both numerical (with increasing resolution) and analytical, were done after their proposal (for a more detailed discussion see e.g., Hess et al. 1999; Klypin et al. 2001; Bullock et al. 2001; Fukushige & Makino 2001, 2003; Mchet & Heft 2003; Zhao et al. 2003).

Generally speaking, the NFW density profile may be considered as a special case of the 5-parameter family (Hernquist 1990; Zhao 1996, 1997):

$$\rho\left(\frac{r}{r_0}\right) = \frac{\rho_0}{(r/r_0)^\gamma [1 + (r/r_0)^\alpha]^\chi} \quad ; \quad \chi = \frac{\beta - \gamma}{\alpha} \quad ; \quad (1)$$

related to the choice $(\alpha, \beta, \gamma) = (1, 3, 1)$, where ρ_0 and r_0 are a scaling density and a scaling radius, respectively ¹.

¹To the knowledge of the authors, the family of density profiles expressed by Eq. (1)

The density profile, expressed by Eq. (1), reduces to a power-law both towards the centre, $r \rightarrow 0$, and towards infinite, $r \rightarrow +\infty$, where the exponent equals $-\gamma$ and $-\beta$, respectively. It may be conceived as a generalized power-law and, in the following, it shall be quoted as GPL density profile. On the other hand, matter distribution within a simulated dark matter halo, in the following, shall be quoted as SDH density profile.

For fixed exponents, one among the two remaining free parameters, the scaling density and the scaling radius, may be related to the mass and the radius of the virialized region. For further details see e.g., NFW; Bullock et al. (2001); Rasia et al. (2004).

Some doubts on the “universality” of the NFW density profile were cast by latter investigations. There are main orders of reasons against the idea of a universal, NFW density profile, which can be briefly summarized as follows.

- (i) A steeper slope in the central regions (e.g., Fukushige & Makino 1997, 2001, 2003; Moore et al. 1998, 1999; Ghigna et al. 2000; but see Navarro et al. 2004, for a different point of view).
- (ii) A non universal slope in the central regions, which depends on the power spectrum of the initial density perturbation (Syer & White 1998), or on the mass (Jing & Suto 2000; Ricotti 2003). Additional support to this idea is provided by recent, high-resolution simulations (e.g., Fukushige et al. 2004; Navarro et al. 2004).
- (iii) A certain degree of degeneracy with regard to the exponents, (α, β, γ) , in fitting various GPL to SDH density profiles, in the whole range of resolved scales (e.g., Klypin et al. 2001).
- (iv) Different criterions in fitting GPL to SDH density profiles, such as minimizing the maximum fractional deviations of the fit, $\max |\log(\rho_{GPL}/\rho_h) - \log(\rho_{SDH}/\rho_h)|$ (e.g., Klypin et al. 2001); the sum of the squares of

was first defined by Hernquist [1990, Eq. (43) therein], even if his attention was restricted to the special case, $(\alpha, \beta, \gamma) = (1, 4, 1)$ which, in turn, was earlier proposed by Kuzmin & Veltmann (1973). A family of density profiles including the special case studied by Hernquist, the so called γ models, where $(\alpha, \beta, \gamma) = (1, 4, \gamma)$, was given independently by Dehnen (1993) and Tremaine et al. (1994). A detailed investigation of general (α, β, γ) models was performed by Zhao (1996, 1997).

absolute²logarithmic residuals, $\chi^2 = \sum [\log(\rho_{GPL}/\rho_h) - \log(\rho_{SDH}/\rho_h)]^2$ (e.g., Bullock et al. 2001); the sum of squares of relative residuals, $\sum [(\rho_{SDH}/\rho_h - \rho_{GPL}/\rho_h)/(\rho_{GPL}/\rho_h)]^2$ (e.g., Fukushige & Makino 2003, 2004), where ρ_h is a normalization value. For a more detailed discussion see e.g., Tasitsiomi et al. (2004).

- (v) A gentler slope in the central regions ($\gamma < 1$) and a steeper slope sufficiently far from the centre ($\beta > 3$), under reasonable boundary conditions such as a finite halo mass and force-free halo centre, and a vanishing density at infinite distance (Mücket & Hoeft 2003). Additional support to this idea is provided by recent high-resolution simulations (Navarro et al. 2004).
- (vi) A gentler slope in the central regions ($\gamma \lesssim 1$) to be consistent with rotation curves, deduced from the observations, of low surface brightness galaxies (McGaugh & de Blok 1988; de Blok et al. 2001), the Galaxy (Binney & Evans 2001), and dwarf galaxies (van den Bosch & Swaters 2001). For a more detailed discussion, see Mücket & Hoeft (2003). In addition, the validity of the Jeans equation implies $1 \leq \gamma \leq 3$ for dark matter haloes (Hansen 2004), unless the effects of the baryonic component are taken into consideration (El-Zant et al. 2004; Hansen 2004).
- (vii) A discrepancy with the dark matter distribution required to ensure hydrostatic equilibrium of gas, deduced from measured X-ray brightness profiles, in clusters of galaxies (Arieli & Rephaeli 2003).

Though the resolution of numerical simulations is increasingly high, still there is no general consensus, or insufficient investigation, about some questions concerning dark matter halo density profiles, namely: (1) definition and formulation of universal density profiles (e.g., Huss et al. 1999; Bullock et al. 2001); (2) connection between GPL and SDH density profiles; (3) dependence of GPL density profiles on the three exponents, (α, β, γ) and the two scaling parameters, (r_0, ρ_0) ; (4) extent to which two or more GPL density profiles fit the results of numerical simulations (e.g., Klypin et al. 2001; Fukushige

²The term “absolute” here has not to be intended as “absolute value”, but as opposite to “relative”. More precisely, $y_i - y(x_i)$ is an absolute residual, while $[y_i - y(x_i)]/y(x_i)$ is the corresponding relative residual.

& Makino 2001, 2003); (5) degree of degeneration of the three exponents in fitting GPL to SDH density profiles (e.g., Klypin et al. 2001).

The hierarchical collapse of dark matter into virialized haloes is likely to have played a key role in the formation of large-scale objects, such as galaxies and clusters of galaxies. The halo profile has a direct dynamical role in determining the observable parameters of the baryonic subsystems. Therefore further investigation on the above raised questions appears to be important.

To this aim, in fitting GPL to SDH density profiles, both a nonlinear least-absolute values and a nonlinear least-squares method are used in the current paper. The related boundary condition is that both the mass and the radius of the virialized region are determined by the computer outputs and the choice of the cosmological parameters. The main features of GPL and SDH density profiles are outlined in sections 2 and 3, respectively. A comparison between GPL and SDH density profiles is performed in section 4. Nonlinear least-absolute values and least-squares fits are outlined in section 5. The subject of section 6 is an application to a sample of 17 SDHs and the related mean density profile, on the scale of clusters of galaxies, taken from Rasia et al. (2004). The results are then discussed. Some concluding remarks are drawn in section 7. Further investigation on a few special arguments is made in the Appendix.

2 GPL density profiles

Plotting GPL density profiles on a logarithmic plane, ($\log \xi$, $\log f$), necessarily implies use of dimensionless coordinates, defined as:

$$\xi = \frac{r}{r_0} ; \quad f(\xi) = \frac{\rho}{\rho_0} ; \quad (2)$$

where the scaled radius, ξ , can be related to density profiles where the isopycnic surfaces i.e. constant density, are similar and similarly placed ellipsoids. For further details, see Caimmi & Marmo (2003). Accordingly, Eq. (1) reduces to:

$$f(\xi) = \frac{1}{\xi^\gamma (1 + \xi^\alpha)^\chi} ; \quad \chi = \frac{\beta - \gamma}{\alpha} ; \quad (3)$$

independent of the scaling parameters.

The special choice:

$$\rho^\dagger = 2^\chi \rho_0 \quad ; \quad r^\dagger = r_0 \quad ; \quad (4)$$

translates Eq. (3) into:

$$f(\xi) = \frac{2^\chi}{\xi^\gamma (1 + \xi^\alpha)^\chi} \quad ; \quad \chi = \frac{\beta - \gamma}{\alpha} \quad ; \quad (5)$$

which has an immediate interpretation, as:

$$f(1) = 1 \quad ; \quad \rho(r^\dagger) = \rho^\dagger \quad ; \quad (6)$$

the scaling density, ρ^\dagger , coincides with the density on an isopycnic surface, where the radius equals the scaling radius, $r = r^\dagger$. For further details, see Caimmi & Marmo (2003).

Scaled GPL density profiles, expressed by Eq. (3), include ∞^2 GPL density profiles, expressed by Eq. (1), for the whole, allowed set of scaling parameters, (r_0, ρ_0) . A similar situation occurs for polytropes (e.g., Caimmi 1980).

As Eqs. (2) and (3) imply null density at infinite radius, the mass distribution has necessarily to be ended at an assigned isopycnic surface, which defines a truncation radius, R . The mass within the truncation isopycnic surface is (Caimmi & Marmo 2003):

$$M = M(R) = \frac{4\pi}{3} r_0^3 \rho_0 \nu_{mas} = M_0 \nu_{mas} \quad ; \quad (7)$$

where M_0 is a scaling mass and the profile factor, ν_{mas} , has the explicit expression:

$$\nu_{mas} = 3 \int_0^\Xi f(\xi) \xi^2 d\xi \quad ; \quad (8)$$

and the integration is carried up to:

$$\Xi = \frac{R}{r_0} \quad ; \quad (9)$$

which may be conceived as a scaled, truncation radius.

The logarithmic GPL density profile, deduced from Eq. (3), is:

$$\log f = -\gamma \log \xi - \chi \log(1 + \xi^\alpha) \quad ; \quad (10)$$

it can be seen that the first and the third logarithmic derivative, calculated at $\log \xi = 0$ i.e. $r = r_0$, yields:

$$\left(\frac{d \log f}{d \log \xi} \right)_{\log \xi=0} = -\frac{1}{2}(\gamma + \beta) \quad ; \quad (11)$$

$$\left(\frac{d^3 \log f}{d(\log \xi)^3} \right)_{\log \xi=0} = 0 \quad ; \quad (12)$$

which discloses the geometrical meaning of the scaling radius.

Geometrical meaning of the scaling radius in GPL density profiles

With regard to logarithmic GPL density profiles, the maximum slope variation rate occurs at the scaling radius, $\log \xi = \log(r/r_0) = 0$, where the slope equals the mean slope of the related asymptotes, $-\gamma$ and $-\beta$, respectively.

In the special case of NFW density profiles, $\gamma = 1$, $\beta = 3$, and the slope at the scaling radius equals -2 (e.g., Bullock et al. 2001; Klypin et al. 2001; Hiotelis 2003). For a more detailed discussion, see Caimmi & Marmo (2003).

In the limit of negligible values of the scaled radius, ξ , with respect to unity, Eq. (10) reduces to:

$$\log f = -\gamma \log \xi \quad ; \quad \xi \ll 1 \quad ; \quad (13)$$

which represents, in the logarithmic plane ($\mathcal{O} \log \xi \log f$), a straight line with slope equal to $-\gamma$ and intercept equal to 0.

In the limit of preponderant values of the scaled radius, ξ , with respect to unity, Eq. (10) reduces to:

$$\log f = -\beta \log \xi \quad ; \quad \xi \gg 1 \quad ; \quad (14)$$

which represents, in the logarithmic plane ($\mathcal{O} \log \xi \log f$), a straight line with slope equal to $-\beta$ and intercept equal to 0.

It can easily be seen that the straight lines, expressed by Eqs. (13) and (14), meet at the origin and, in addition, represent the asymptotes of the logarithmic GPL density profile, expressed by Eq. (10). The special cases related to NFW and MOA (Moore et al. 1999) logarithmic density profiles, are plotted in Fig. 1. The above results hold for $\alpha > 0$. The case $\alpha < 0$ makes the asymptotes change one into the other. The limiting case $\alpha = 0$ makes either a vanishing density ($\beta \neq \gamma$) or the asymptotes coincide i.e. the curve reduces to a straight line ($\beta = \gamma$).

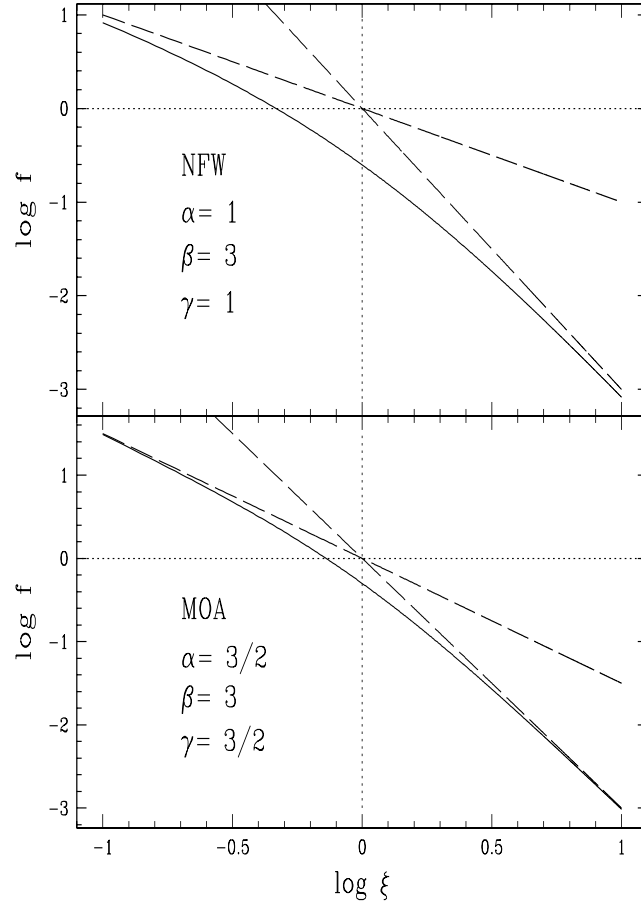


Figure 1: Logarithmic NFW (top) and MOA (bottom) density profiles (full curves), with their asymptotes (dashed lines), in the plane $(\log \xi, \log f)$.

3 SDH density profiles

Dark matter haloes simulations need three basic ingredients, namely: (i) a cosmological model with fixed values of the parameters; (ii) an environment with defined initial conditions; and (iii) an assigned computer code. The density profile during the evolution, is calculated through the following steps: (1) determine the centre of mass of the halo; (2) count the particles (bound to the halo) within spherical shells, centered on the centre of mass, and equally spaced in logarithmic distance i.e. $\log(r_{i+1}/r_i) = \text{const}$; (3) evaluate the mean density within each shell. For further details see e.g., NFW; Klypin et al. (2001); Bullock et al. (2001); Fukushige & Makino (2001, 2003).

Simulated haloes are characterized by a “virial” parameter, either the virial mass, M_{vir} , or the virial radius, r_{vir} , defined such that the mean density inside the virial radius is Δ_{vir} times the mean matter universal density, $\rho_h = \rho_{\text{crit}}\Omega_m$, at that redshift:

$$M_{\text{vir}} = \frac{4\pi}{3} \Delta_{\text{vir}} \rho_{\text{crit}} \Omega_m r_{\text{vir}}^3 ; \quad (15)$$

where $\rho_{\text{crit}} = 3H^2/(8\pi G)$ is the critical density for closure of the Universe. The critical overdensity at virialization, Δ_{vir} , is motivated by the spherical collapse model: it is below two hundreds for an Einstein-de Sitter cosmology, and exceeds three hundreds for a flat Λ CDM cosmology where $\Omega_m \approx 0.3$, at $z = 0$ (e.g., Bullock et al. 2001).

Plotting SDH density profiles on a logarithmic plane, ($\text{O log } \eta \text{ log } \psi$), necessarily implies use of dimensionless coordinates, defined as:

$$\eta = \frac{r}{r_{\text{vir}}} ; \quad \psi(\eta) = \frac{\rho}{\rho_h} ; \quad \rho_h = \rho_{\text{crit}} \Omega_m ; \quad (16)$$

without loss of generality.

An upper limit to the domain of SDH density profiles follows from the definition of virial radius: regions placed outside are still falling in, and their macroscopic kinetic energy has still to be converted into peculiar energy (e.g., Cole & Lacey 1996; NFW).

A lower limit to the domain of SDH density profiles is put by the occurrence of numerical artifacts (mainly two-body relaxation) in the central regions, within about $0.01r_{\text{vir}}$ (e.g., Bullock et al. 2001; Fukushige & Makino

2001, 2003, 2004; Navarro et al. 2004) or even less (e.g., Diemand et al. 2004; Reed et al. 2005).

Accordingly, SDH density profiles appear to be closely related to the virialized region in the range:

$$-2 < \log \eta < 0 \quad ; \quad (17)$$

which shall be assumed in the following. A typical SDH density profile on the scale of cluster of galaxies, taken from a sample of 17 simulated haloes (Rasia et al. 2004), is represented in Fig. 2. Also plotted therein are the best linear fits, determined by use of a least-squares fit to simulated data, within the γ -region, $-2 < \log \eta < -1$, and the β -region, $-1 < \log \eta < 0$, respectively. For further details, see Appendix A.

4 Comparison between GPL and SDH density profiles

A comparison between GPL and SDH density profiles necessarily implies that the truncation radius, and the mass enclosed within the truncation isopycnic surface, do coincide with the virial radius and the virial mass, $R = r_{\text{vir}}$ and $M = M_{\text{vir}}$, respectively. Then the combination of Eqs. (7) and (15) yields:

$$\frac{\rho_0}{\rho_h} = \frac{\Delta_{\text{vir}} \xi_{\text{vir}}^3}{\nu_{\text{mas}}} \quad ; \quad (18)$$

$$\xi_{\text{vir}} = \frac{r_{\text{vir}}}{r_0} \quad ; \quad (19)$$

where the scaled virial radius, ξ_{vir} , is usually defined as concentration in the special case of NFW density profiles (NFW). With regard to a generic GPL density profile, there are several definitions of concentration (e.g., Klypin et al. 2001). Throughout this paper we shall define the concentration as the scaled virial radius i.e. the ratio of the virial radius to the radius where the logarithmic slope of the density profile equals the mean slope of the two asymptotes, and the slope variation rate is maximum, according to Eqs. (11) and (12), respectively.

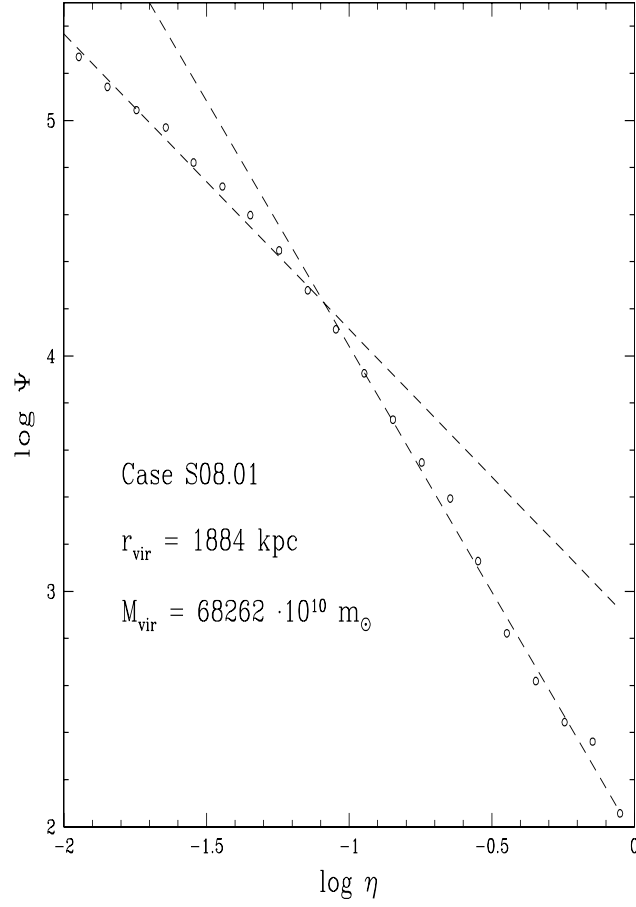


Figure 2: Logarithmic SDH density profile (open circles) for a typical dark matter halo on the scale of clusters of galaxies. The virialized region is safely represented in the range $-2 < \log \eta < 0$. Also plotted are the best linear fits (dashed), determined by use of a least-squares fit to simulated data, within the γ -region, $-2 < \log \eta < -1$, and the β -region, $-1 < \log \eta < 0$, respectively.

The comparison of scaled GPL density profiles, expressed by Eqs. (2), with scaled SDH density profiles, expressed by Eqs. (16), yields:

$$\xi = \xi_{\text{vir}}\eta \quad ; \quad f = \frac{\rho_h}{\rho_0}\psi \quad ; \quad (20)$$

where ξ_{vir} is defined by Eq. (19). Accordingly, a generic, scaled GPL density profile, expressed by Eq. (3), takes the equivalent form:

$$\psi(\eta) = \frac{\rho_0/\rho_h}{(\xi_{\text{vir}}\eta)^\gamma [1 + (\xi_{\text{vir}}\eta)^\alpha]^\chi} \quad ; \quad \chi = \frac{\beta - \gamma}{\alpha} \quad ; \quad (21)$$

and the related, logarithmic GPL density profile, is deduced by use of Eq. (18). The result is:

$$\begin{aligned} \log \psi &= \log \Delta_{\text{vir}} - \log \nu_{\text{mas}} + 3 \log \xi_{\text{vir}} \\ &\quad - \gamma \log \xi_{\text{vir}} - \gamma \log \eta - \chi \log [1 + (\xi_{\text{vir}}\eta)^\alpha] \quad ; \end{aligned} \quad (22)$$

which depends on three exponents, (α, β, γ) , and two scaling parameters, (r_0, ρ_0) . On the other hand, the scaled mass, ν_{mas} , is defined by Eqs. (8) and (9); the virial radius, r_{vir} , is known from the computer run; and the critical overdensity, Δ_{vir} , is determined by the cosmological model.

According to Eqs. (2), (11), (12), and (20), the maximum variation in slope occurs at $r = r_0$ i.e. $\log \xi = 0$ i.e. $\log \eta = -\log \xi_{\text{vir}}$. Then Eqs. (11) and (12) translate into:

$$\left(\frac{d \log \psi}{d \log \eta} \right)_{\log \eta = -\log \xi_{\text{vir}}} = -\frac{1}{2}(\gamma + \beta) \quad ; \quad (23)$$

$$\left(\frac{d^3 \log \psi}{d(\log \eta)^3} \right)_{\log \eta = -\log \xi_{\text{vir}}} = 0 \quad ; \quad (24)$$

where the slope at $\log \eta = -\log \xi_{\text{vir}}$ equals the mean slope of the related asymptotes, $-\gamma$ and $-\beta$, respectively.

In the limit of negligible values of the scaled radius, $\xi_{\text{vir}}\eta$, with respect to unity, Eq. (22) reduces to:

$$\begin{aligned} \log \psi &= \log \Delta_{\text{vir}} - \log \nu_{\text{mas}} + 3 \log \xi_{\text{vir}} \\ &\quad - \gamma \log \xi_{\text{vir}} - \gamma \log \eta \quad ; \quad \xi_{\text{vir}}\eta \ll 1 \quad ; \end{aligned} \quad (25)$$

which represents, in the logarithmic plane ($\text{O log } \eta \text{ log } \psi$), a straight line with slope equal to $-\gamma$ and intercept equal to $\log \Delta_{\text{vir}} - \log \nu_{\text{mas}} + (3 - \gamma) \log \xi_{\text{vir}}$.

In the limit of preponderant values of the scaled radius, $\xi_{\text{vir}}\eta$, with respect to unity, Eq. (22) reduces to:

$$\begin{aligned} \log \psi &= \log \Delta_{\text{vir}} - \log \nu_{\text{mas}} + 3 \log \xi_{\text{vir}} \\ -\beta \log \xi_{\text{vir}} - \beta \log \eta &; \quad \xi_{\text{vir}}\eta \gg 1 ; \end{aligned} \quad (26)$$

which represents, in the logarithmic plane ($\text{O log } \eta \text{ log } \psi$), a straight line with slope equal to $-\beta$ and intercept equal to $\log \Delta_{\text{vir}} - \log \nu_{\text{mas}} + (3 - \beta) \log \xi_{\text{vir}}$.

It can easily be seen that the straight lines, expressed by Eqs. (25) and (26), meet at the point $(\log \eta, \log \psi) = [\log(r_0/r_{\text{vir}}), \log(\rho_0/\rho_h)]$, where Eqs. (18) and (2) have been used. In addition, the above mentioned straight lines represent the asymptotes of the logarithmic GPL density profile, expressed by Eq. (22). Special cases related to NFW and MOA (Moore et al. 1999) logarithmic density profiles, are plotted in Fig. 3.

5 The RFSM5 method

Given a set of SDH density profiles, one is left with the problem of fitting a GPL density profile to each simulation and to the average on the whole set. To this respect, nonlinear fits shall be used, minimizing the sum of both absolute values and squares of absolute logarithmic residuals, $R_i = \log \psi_{\text{SDH}}(\eta_i) - \log \psi_{\text{GPL}}(\eta_i)$, used in the literature (e.g., Klypin et al. 2001; Bullock et al. 2001).

Strictly speaking, the problem reduces to a search of extremum points of minimum, with regard to a function, $Y = F(X_1, X_2, X_3, X_4, X_5)$, which represents a 5-dimension hypersurface in a 6-dimension hyperspace. In general, no point of minimum can exist within the domain, if bounded, or a finite number, or infinite. If two or more minima are present, then degeneracy occurs. Owing to an intrinsic difficulty related to the above mentioned analytical procedure, a numerical alternative shall be exploited.

More specifically, a 5-dimension hypergrid made of 10^5 points is placed around a fiducial minimum, and the sum of both absolute values and squares of absolute logarithmic residuals, $\sum |R_i|$ and $\sum R_i^2$, respectively, are evaluated at each point, and finally two (in general) distinct minima are localized. Then a new iteration is performed, with respect to a new hypergrid, centered near

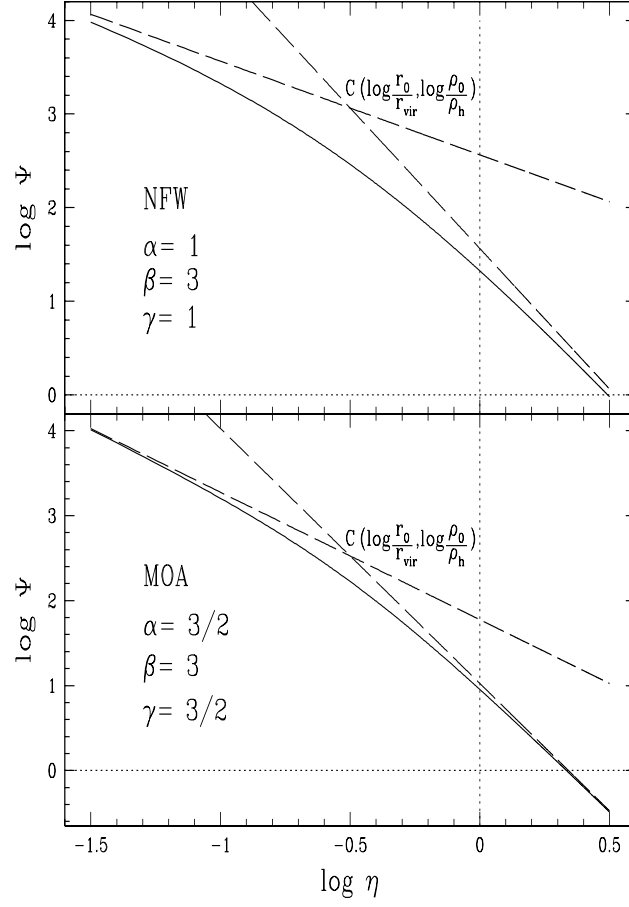


Figure 3: Logarithmic NFW (top) and MOA (bottom) density profiles (full curves), with their asymptotes (dashed lines), in the plane ($\log \eta$, $\log \psi$). Values of r_0/r_{vir} and ρ_0/ρ_h have been arbitrarily chosen.

the minima, where the size has been reduced and superpositions on nodes of earlier hypergrids have been avoided. For the calculations made in the current paper, three iterations have been revealed to be sufficient.

In dealing with the hypergrid, it would be better to use parameters with an immediate geometrical meaning, instead of their analytical counterparts, $(r_0, \rho_0, \alpha, \beta, \gamma)$. To this aim, the logarithmic GPL density profile, expressed by Eq. (22), has to be studied in detail, which is made in Appendix A. The geometrical parameters to be used, $(x_C, y_C, b, b_\beta, b_\gamma)$, are the coordinates of the intersection of the asymptotes, and the vertical intercepts of the curve and the asymptotes, respectively.

In summary, the procedure outlined above acts along the following steps.

- (i) Select a set of SDH density profiles, related to an assigned computer code and a specified cosmological model.
- (ii) Determine, for each SDH density profile, the GPL density profiles which minimize the sum of absolute values and/or squares of absolute logarithmic residuals, using a 5-dimension hypergrid in the 5-dimension hyperspace $(Ox_C y_C b b_\beta b_\gamma)$.
- (iii) Perform the desired number of iterations around the minima, using a hypergrid with same number of points (but none in common), and reduced in size, in respect of its earlier analogon.
- (iv) Define a mean SDH density profile, over the whole set of simulations, and repeat the procedure used for a single SDH density profile.

The result consists in a one-to-one correspondence between SDH density profiles, including the related mean, and GPL density profiles which minimize the sum of absolute values and/or squares of absolute logarithmic residuals, in connection with the hypergrid used. In the following, the above mentioned procedure shall be quoted as RFSM5 (Residual Functions Sum Minimization within a 5-dimension hyperspace) method. The functions used in the current paper are the absolute value and the square of the absolute logarithmic residual.

6 An application to SDHs on the scale of cluster of galaxies

Using a RFSM5 method, GPL density profiles are fitted to a sample of 17 SDH density profiles, on the scale of cluster of galaxies within a flat Λ CDM cosmology (Rasia et al. 2004, hereafter quoted as RTM). The values of the cosmological parameters used therein are: $\Omega_\Lambda = 0.7$; $\Omega_m = 0.3$; $\Omega_b = 0.03$; $h = 0.7$; $\sigma_8 = 0.9$; where the symbols have their usual captions (e.g., Klypin et al. 2001; Bullock et al. 2001) and, in particular, the indices m and b denote all matter (dark + baryonic) and baryonic, respectively. For a detailed discussion on the computer code, initial conditions, the resolution issues, and the way of finding the halo centre, see RTM and further references therein.

Simulations include both dark and baryonic matter, but only the former is relevant to the aim of the current paper. Accordingly, the baryonic matter shall not be considered, and all the parameters shall be intended as related to the dark matter halo.

The definition of the virialized region within each halo, via Eq. (15), needs the knowledge of the critical overdensity at virialization, Δ_{vir} . With regard to total (dark + baryonic) matter, it depends on the cosmological model (e.g., Bullock et al. 2001) and, in the case under discussion, $(\Delta_{\text{vir}})_m = 323$ at $z = 0$, where all the sample haloes may be considered as virialized to an acceptable extent (RTM).

If only the dark matter is considered, then $(\Delta_{\text{vir}})_d = \Delta_{\text{vir}} = \zeta(\Delta_{\text{vir}})_m$, where ζ is the fraction of dark matter in each density perturbation, and averaging over the whole sample yields $\zeta = 0.907$ (RTM). Accordingly, the value:

$$\Delta_{\text{vir}} = 0.907 \cdot 323 = 292.961 \quad ; \quad (27)$$

can be used to an acceptable extent ³.

As clearly pointed out in RTM, owing to the random criterion used for selection, their sample haloes are characterized by varying dynamical proper-

³The above value of the critical overdensity was deduced from an earlier, unpublished version of RTM. It is slightly different from $\Delta_{\text{vir}} = 0.903 \cdot 323.7625 = 292.3576$, deduced from the current version, which appeared when the calculations were performed in this paper. As the relative difference amounts to about 0.2%, the calculations were not repeated using the latter value of the critical overdensity.

ties: at the present time, some are more relaxed, while others are dynamically perturbed. The surrounding environment can also be quite different: some selected clusters are more isolated, while others are interacting with the surrounding cosmic web. Accordingly, the sample is expected to be good enough to provide unbiased conclusions, and the related modelling may be thought of as representative of an average cluster, in an average environment and dynamical configuration.

6.1 Individual SDH density profiles

The main features of sample haloes at $z = 0$ are listed in Tab. 1. The mass, M_{vir} , has been taken from RTM, while the mass, M'_{vir} , has been deduced from Eq. (15). The apparent discrepancy between M_{vir} and M'_{vir} is owing to two different sources. First, a systematic contribution takes origin from the uncertainty on Δ_{vir} and, second, a random contribution arises from the uncertainty on r_{vir} , in both cases with regard to Eq. (15). An additional random contribution is related to averaging the fraction of dark matter over the whole sample, with regard to Eq. (27).

The relative difference, $|1 - M'_{\text{vir}}/M_{\text{vir}}|$, is less than one percent in all cases except 9, where it is less than one and half percent. Then the virial mass can be evaluated, to a good extent, by use of Eq. (15), taking the virial radius from the results of simulations. It is worth mentioning that the RFSM5 method is independent of the value of the virial mass, while a change in the value of the virial radius makes SDH density profiles systematically shift along the horizontal direction, see Fig. 2.

6.2 Averaged SDH density profiles

Given a set of logarithmic SDH density profiles, the mean SDH density profile is obtained by averaging over the whole set the values related to each logarithmic radial bin, in the range of interest, expressed by Eq. (17). The value of the critical overdensity at virialization, Δ_{vir} , is fixed by Eq. (27), then a single free parameter remains: the virial radius, r_{vir} , which allows the calculation of the virial mass, M_{vir} . The related values are determined by averaging over the whole sample, using the data listed in Tab. 1, and inserting

case	run	type	N	r_{vir}	M_{vir}	M'_{vir}
1	<i>S01.02</i>	<i>R</i>	282574	1953	76330	76040
2	<i>S02.10</i>	<i>M</i>	278569	2305	125400	125010
3	<i>S02.11</i>	<i>M</i>	85159	1553	38340	38234
4	<i>S03.05</i>	<i>R</i>	294373	2347	132500	131970
5	<i>S04.01</i>	<i>R</i>	179681	1991	80820	80565
6	<i>S04.07</i>	<i>R</i>	146386	1860	65850	65686
7	<i>S05.02</i>	<i>M</i>	318653	2197	108700	108249
8	<i>S06.01</i>	<i>M</i>	427583	2470	153800	153825
9	<i>S06.03</i>	<i>M</i>	166855	1796	60020	59136
10	<i>S07.01</i>	<i>R</i>	275259	1691	49600	49359
11	<i>S07.03</i>	<i>R</i>	158345	1407	28530	28433
12	<i>S08.01</i>	<i>R</i>	190453	1884	68600	68262
13	<i>S08.04</i>	<i>R</i>	101482	1529	36560	36489
14	<i>S09.03</i>	<i>R</i>	159330	1913	71690	71463
15	<i>S09.14</i>	<i>R</i>	107229	1675	48250	47971
16	<i>S10.03</i>	<i>R</i>	58734	1524	36060	36132
17	<i>S10.07</i>	<i>R</i>	71937	1628	44170	44045

Table 1: Main features of sample haloes at $z = 0$. Column captions: 1 - case; 2 - computer run; 3 - type (*R* - safely relaxed; *M* - safely a major merger occurring); 4 - number of dark matter particles within the virial radius; 5 - virial radius (h^{-1} kpc); 6 - virial mass ($h^{-1}10^{10}M_{\odot}$); 7 - virial mass deduced from Eq.(15). Both virial radii and virial masses are normalized to the dimensionless Hubble parameter at the current time, h .

the mean value of the virial radius into Eq. (15). The result is:

$$\bar{r}_{\text{vir}} = 1866 \, h^{-1} \, \text{kpc} \quad ; \quad \bar{M}_{\text{vir}} = 66330 \, h^{-1} \, 10^{10} \text{M}_{\odot} \quad ; \quad (28)$$

and the application of a RFSM5 method yields best fitting GPL density profiles, with radius and mass equal to \bar{r}_{vir} and \bar{M}_{vir} , respectively.

A mean virial radius has been preferred in place of a mean concentration (RTM) for the following reasons. First, virial radii are independent of GPL density profiles, contrary to concentrations, or velocity profiles, which should be calculated for any choice of the fitting profile. Second, the range of virial radii, $1407 \leq r_{\text{vir}}/(h^{-1}\text{kpc}) \leq 2470$, corresponds to relative errors of about 25% and 33%, respectively, with regard to a mean value, $\bar{r}_{\text{vir}} = 1866 \, h^{-1}\text{kpc}$. On the other hand, the range of concentrations (calculated for NFW density profiles), $5 \leq \xi_{\text{vir}} \leq 10$, corresponds to relative errors of about 32% and 37%, respectively, with regard to a mean value, $\bar{\xi}_{\text{vir}} = 7.2976$. Then the average of the virial radius should be preferred to this respect.

Having in our hands a SDH density profile averaged over the sample, listed in Tab. 1, and a value of virial radius and virial mass, expressed by Eq. (28), we are left with the search of a best fitting GPL density profile. To this aim, six alternatives are exploited. The first one consists in the mere application of the RFSM5 method to the mean SDH density profile.

Among the remaining five, three allow to fix the exponents in the GPL density profile, expressed by Eq. (1), and then minimize the sum of absolute values and/or squares of absolute logarithmic residuals, with respect to a single free parameter, the scaling radius, r_0 (e.g., Zhao et al. 2003). Accordingly, the minimization is performed using a 2-dimension grid. The related procedure shall be quoted as RFSM2 (Residual Functions Sum Minimization within a 2-dimension space) method. The function used in the current paper is the absolute value and/or the square of the absolute logarithmic residual. The following special GPL density profiles are selected: NFW, MOA, and a best fitting profile deduced from both density and velocity distributions in sample haloes (RTM), hereafter quoted as RTM density profile⁴. The related values of the exponents are $(\alpha, \beta, \gamma) = (1, 3, 1)$, $(3/2, 3, 3/2)$, $(1, 5/2, 1)$, respectively.

Finally, the last two alternatives among the six mentioned above, consist in calculating the mean values of the geometrical parameters, $(x_C, y_C, b, b_{\beta}, b_{\gamma})$,

⁴It is worth mentioning that a different normalization has been used here for the scaling density, $\rho_0 = (\xi_{\text{vir}})^{5/2}(\rho_0)_{\text{RTM}}$.

over the whole sample of best fitting, GPL density profiles, with regard to the minimization of the sum of absolute values and squares of absolute logarithmic residuals, respectively.

6.3 Results

As outlined in section 5, a RFSM5 method has been applied to each sample halo, listed in Tab. 1, and to the related, averaged SDH density profile, which has been defined above. In addition, a RFSM2 method has been applied to the mean SDH density profile, in the special case of NFW, MOA, and RTM density profiles. The values of the exponents, α , χ , β , γ , the scaled radius, ξ_{vir} , the scaling radius, r_0 , the scaling density, ρ_0 , and the sum of residual functions at the fiducial minimum, $\sum f(R_i)$, where $f(R_i) = |R_i|$ and $f(R_i) = R_i^2$, are listed in Tabs. 2 and 3, respectively. The following conclusions are deduced.

- (i) In general, different GPL density profiles best fit to an assigned SDH density profile, with regard to the minimization of the sum of absolute values or squares of absolute logarithmic residuals, respectively. The best fitting GPL density profiles in the two above mentioned alternatives, are closer each to the other in dealing with the mean geometrical parameters, than with the mean SDH density profile.
- (ii) The values of the exponents, (α, β, γ) , appearing in Eq. (1), and deduced from the geometrical parameters averaged over the whole halo sample, $(\bar{x}_C, \bar{y}_C, \bar{b}, \bar{b}_\beta, \bar{b}_\gamma)$, are $(\bar{\alpha}, \bar{\beta}, \bar{\gamma}) \approx (0.6, 3.1, 1.0)$.
- (iii) With regard to the mean SDH density profile, the GPL density profiles which best minimize the sum of squares of absolute logarithmic residuals, occur in the following order of accuracy: (1) application of a RFSM5 method (ADP); (2) density profile related to mean values of geometrical parameters (AGP); (3) RTM; (4) MOA; (5) NFW. The best minimization of the sum of absolute values of absolute logarithmic residuals, implies the same order as above, but with AGP and RTM density profiles interchanged.

The SDH density profiles related to the current sample, listed in Tab. 1, and the related mean SDH density profile, are plotted in Fig. 4 (dots) together

case	α	χ	β	γ	ξ_{vir}	r_0	$10^4 \rho_0$	$\sum R_i $
1	0.74154	3.1652	3.4698	1.1226	3.3884	823.39	0.51314	0.37127
2	0.55959	4.5587	3.3698	0.81879	3.9446	834.78	1.6992	0.67590
3	0.44184	3.7405	2.8307	1.1780	6.6069	335.79	2.6317	0.77869
4	0.45956	3.6948	2.7388	1.0409	7.2577	461.97	2.6930	0.76086
5	0.65993	2.7518	3.0723	1.2563	4.7315	601.14	0.74171	0.45363
6	0.52739	3.2392	2.6766	0.96825	13.884	191.38	7.3923	0.62044
7	0.59587	4.0247	3.4760	1.0778	4.6559	674.11	1.8207	0.57012
8	0.66861	3.9138	3.4748	0.85806	4.1687	846.45	1.3190	0.22446
9	0.56370	3.9028	3.1506	0.95062	6.4565	397.38	3.2377	0.27807
10	0.42473	3.8973	2.7797	1.1139	6.1660	391.78	2.3455	0.47658
11	0.65178	3.7207	3.5506	1.1255	3.2359	621.15	0.67645	0.44895
12	0.66423	3.5417	2.9664	0.61389	7.9433	338.83	3.2752	0.75673
13	0.70250	3.1223	3.1281	0.93462	6.0256	362.50	1.6605	0.58189
14	0.74575	3.2092	3.2130	0.81972	5.1286	532.86	1.2029	0.35644
15	0.82346	2.1323	2.7865	1.0307	6.5313	366.37	0.91250	0.59466
16	0.71709	3.8681	3.7082	0.93443	4.0738	534.43	1.2889	0.43596
17	0.47209	3.1773	2.6513	1.1513	5.7544	404.16	1.1488	0.66217
ADP	0.54955	4.5235	3.3962	0.91034	3.8019	701.18	1.5496	0.12966
AGP	0.60209	3.4021	3.0756	1.0272	5.5083	483.96	1.5422	0.36819
NFW	1	2	3	1	6.35	419.81	0.90131	0.85996
MOA	1.5	1	3	1.5	3.08	865.52	0.093933	0.47639
RTM	1	1.5	2.5	1	13.050	204.28	2.1949	0.32672

Table 2: Parameters of GPL density profiles which (i) minimize the sum of absolute values of logarithmic absolute residuals, using a RFSM5 method with regard to 17 sample haloes listed in Tab.1 (top), and (ii) fit to the mean SDH density profile, to a different extent (bottom). Cases correspond to computer runs in the former alternative, and to GPL density profiles in the latter. The GPL density profile which minimizes the sum of absolute values of absolute logarithmic residuals, using a RFSM5 method with regard to the mean SDH density profile, is denoted as ADP. The GPL density profile defined by geometrical parameters, $(x_C, y_C, b, b_\beta, b_\gamma)$, averaged over their counterparts listed on the top (first 17 rows), is denoted as AGP. The scaling radius, r_0 , and the scaling density, ρ_0 , are expressed in kpc and $10^{10} \text{M}_\odot / \text{kpc}^3$, respectively.

case	α	χ	β	γ	ξ_{vir}	r_0	$10^4 \rho_0$	$\sum R_i^2$
1	0.85979	2.7291	3.4893	1.1429	3.6308	768.43	0.45733	0.012843
2	0.70267	2.6771	2.8238	0.94262	7.1450	460.86	1.4462	0.050984
3	0.50594	3.6824	3.0631	1.2000	4.4668	496.68	1.1755	0.059798
4	0.40157	4.8960	2.9564	0.99023	4.1115	815.48	2.1391	0.044834
5	0.59295	3.2455	3.1244	1.2000	4.7863	594.26	1.0721	0.015935
6	0.50437	2.8516	2.5152	1.0769	16.501	161.03	7.3632	0.033055
7	0.60451	4.1915	3.5715	1.0377	4.2267	742.56	1.7070	0.029137
8	0.66861	3.9138	3.4748	0.85806	4.1687	846.45	1.3190	0.0049367
9	0.58477	3.7717	3.2083	1.0027	5.6234	456.26	2.2399	0.0061089
10	0.43019	3.7611	2.7372	1.1192	6.6374	363.95	2.5132	0.020731
11	0.69931	3.3055	3.4625	1.1509	3.7154	541.00	0.67645	0.017674
12	0.67451	3.0786	2.7795	0.70312	9.1201	363.19	2.8856	0.050487
13	0.68562	3.3840	3.1595	0.83933	6.8234	320.12	2.5718	0.036570
14	0.81937	2.4907	2.9870	0.94621	5.3088	514.77	0.77666	0.012273
15	0.70472	2.8497	2.8694	0.86117	7.6913	311.11	1.9963	0.028821
16	0.74414	3.9381	3.8674	0.93684	3.7154	585.99	1.1226	0.015259
17	0.44450	4.0781	2.8351	1.0224	4.6774	497.23	1.5144	0.057718
ADP	0.56832	4.0722	3.3143	1.0000	3.6308	734.22	1.0238	0.0014983
AGP	0.58866	3.5008	3.0528	0.99204	5.5170	483.20	1.5726	0.0065805
NFW	1	2	3	1	6.44	413.94	0.93151	0.046088
MOA	1.5	1	3	1.5	3.05	874.03	0.091827	0.015492
RTM	1	1.5	2.5	1	13.350	199.69	2.3074	0.0072902

Table 3: Parameters of GPL density profiles which (i) minimize the sum of squares of logarithmic absolute residuals, using a RFSM5 method with regard to 17 sample haloes listed in Tab. 1 (top), and (ii) fit to the mean SDH density profile, to a different extent (bottom). Cases correspond to computer runs in the former alternative, and to GPL density profiles in the latter. The GPL density profile which minimizes the sum of squares of absolute logarithmic residuals, using a RFSM5 method with regard to the mean SDH density profile, is denoted as ADP. The GPL density profile defined by geometrical parameters, $(x_C, y_C, b, b_\beta, b_\gamma)$, averaged over their counterparts listed on the top (first 17 rows), is denoted as AGP. The scaling radius, r_0 , and the scaling density, ρ_0 , are expressed in kpc and $10^{10} \text{M}_\odot/\text{kpc}^3$, respectively.

with their best fitting GPL counterpart (full curves), determined by use of a RFSM5 method in the range defined by Eq. (17). In most cases, GPL density profiles related to the minimization of the sum of absolute values and squares of absolute logarithmic residuals, are virtually indistinguishable, and sometimes coincident.

Different fits to the mean SDH density profile, listed on the lower parts of Tabs. 2 and 3, are represented in Fig. 5, where $\log[(r/r_{\text{vir}})^2(\rho/\rho_h)]$ has been plotted instead of $\log(\rho/\rho_h)$, to make different trends more evident. Curves related to the minimization of the sum of absolute values and squares of absolute logarithmic residuals are virtually indistinguishable with regard to GPL density profiles with fixed exponents: NFW, MOA, and RTM.

The values of some analytical and geometrical parameters, η_{ADP} , related to the best fitting GPL density profile to the mean SDH density profile, are listed in Tabs. 4 and 5 together with their counterparts, $\bar{\eta}$, averaged over the best fitting GPL density profiles to the whole halo sample, via minimization of the sum of absolute values and squares of absolute logarithmic residuals, respectively. Also listed therein are the related standard deviations, $\sigma_s \eta$, the standard deviations from the mean, $\sigma_s \bar{\eta}$, and the standard deviations from the standard deviation from the mean, $\sigma_s \bar{\mu}$, which are expressed as (e.g., Oliva & Terrasi 1976, Chap. V, § 5.6.3):

$$\bar{\eta} = \frac{1}{n} \sum_{i=1}^n \eta_i \quad ; \quad (29)$$

$$\sigma_{s\eta} = \left[\frac{1}{n-1} \sum_{i=1}^n (\eta_i - \bar{\eta})^2 \right]^{1/2} \quad ; \quad (30)$$

$$\sigma_{s\bar{\eta}} = \left[\frac{1}{n} \frac{1}{n-1} \sum_{i=1}^n (\eta_i - \bar{\eta})^2 \right]^{1/2} \quad ; \quad (31)$$

$$\sigma_{s\bar{\mu}} = \frac{\sigma_{s\bar{\eta}}}{\sqrt{2n}} \quad ; \quad \bar{\mu} = \sigma_{s\bar{\eta}} \quad ; \quad (32)$$

where $n = 17$; $\eta = \alpha, \beta, \gamma, \xi_{\text{vir}}, \nu_{\text{mas}}, \log \xi_{\text{vir}}, \log \nu_{\text{mas}}, y_C, b, b_\beta, b_\gamma$; and, owing to Eq. (39), $\log \xi_{\text{vir}} = -x_C$.

The following conclusions are deduced from Tabs. 4 and 5.

- (iv) Values of parameters, η_{ADP} , related to the best fitting GPL density profile to the mean SDH density profile, are different from their coun-

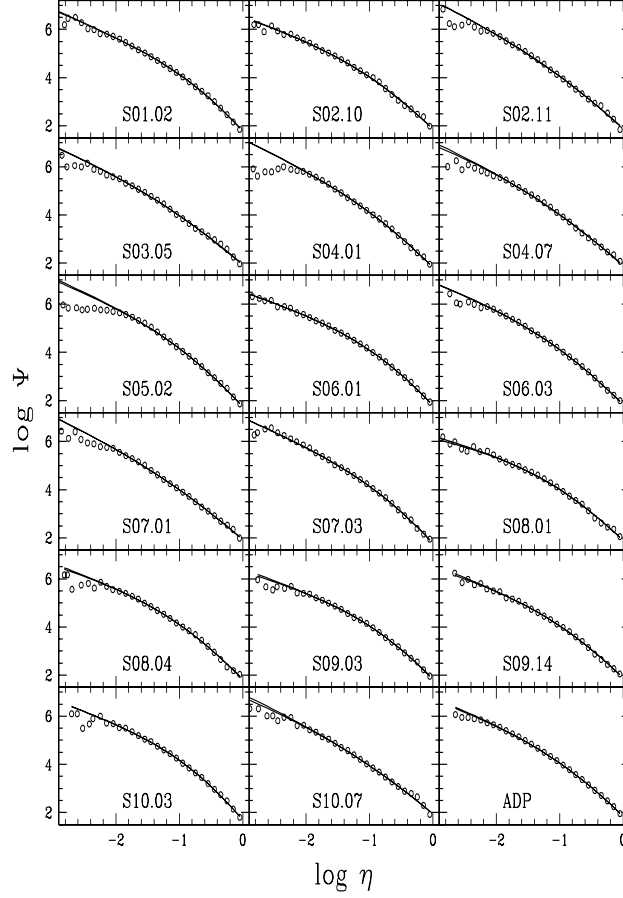


Figure 4: The SDH density profiles related to the current sample, listed in Tab. 1, and the mean SDH density profile, denoted as *ADP* (open circles), together with their best fitting GPL counterparts (full curves), determined by use of a RFSM5 method in the range $-2 < \log(r/r_{\text{vir}}) < 0$. Two curves on each panel correspond to the minimization of the sum of absolute values and squares of absolute logarithmic residuals, respectively. The above mentioned curves are virtually indistinguishable in most cases, and sometimes coincident.

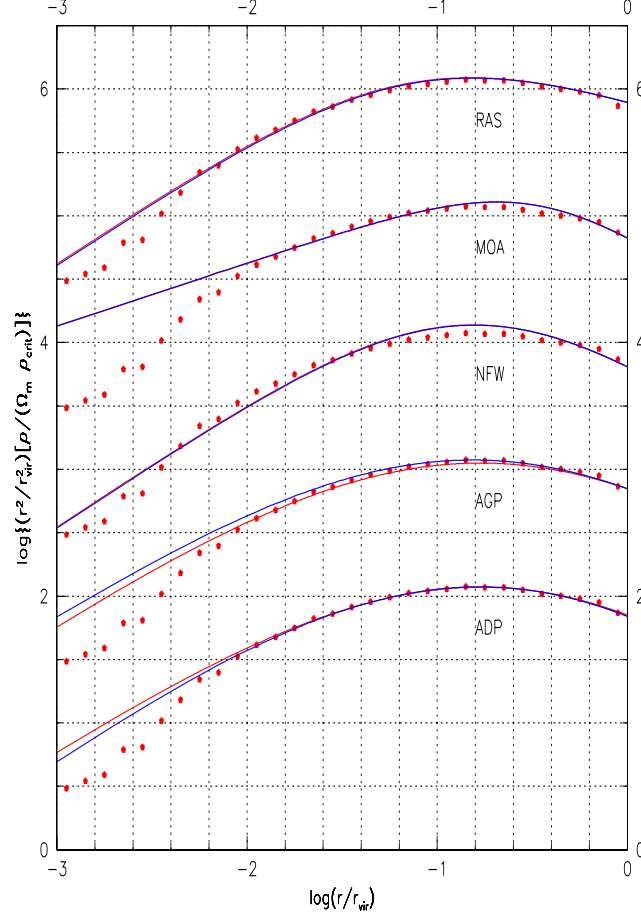


Figure 5: Comparison between different fits (full curves) to the mean SDH density profiles (filled circles), listed on the lower parts of Tabs.2 and 3. The function $\log[(r/r_{\text{vir}})^2(\rho/\rho_h)]$ has been plotted instead of $\log(\rho/\rho_h)$, to make different trends more evident. The vertical scale is related to the lower case. The remaining cases are, in turn, vertically shifted of one unity with respect to their closest counterpart, starting from the lower one, to gain clarity. With regard to case AGP, the upper and the lower curve correspond to the minimization of the sum of absolute values and squares of absolute logarithmic residuals, respectively, and the contrary holds for case ADP. Concerning the remaining cases NFW, MOA, and RTM (labelled here as RAS), the two curves are virtually indistinguishable.

η	η_{ADP}	$\bar{\eta}$	$\sigma_s \eta$	$\sigma_s \bar{\eta}$	$\sigma_s \bar{\mu}$
α	0.54955	0.61292	0.11931	0.028937	0.0049626
β	3.3962	3.1202	0.34247	0.083062	0.014245
γ	0.91034	0.99973	0.16188	0.039261	0.0067332
ξ_{vir}	3.8019	5.8796	2.4766	0.60068	0.10301
ν_{mas}	0.42346	1.4063	1.0804	0.26205	0.044941
$\log \xi_{\text{vir}}$	0.58	0.74102	0.15471	0.037522	0.0064350
$\log \nu_{mas}$	-0.37319	0.050834	0.29116	0.070617	0.012111
y_C	4.58	4.5779	0.29347	0.071178	0.012207
b	1.84	1.8467	0.065779	0.015954	0.0027360
b_β	2.6102	2.2988	0.14859	0.036038	0.0061804
b_γ	4.052	3.8167	0.31970	0.077538	0.013298

Table 4: Comparison between parameters, η_{ADP} , related to the best fitting GPL density profile to the mean SDH density profile, and their counterparts, $\bar{\eta}$, averaged over the best fitting GPL density profiles to the whole halo sample, with regard to the minimization of the sum of absolute values of absolute logarithmic residuals. Also listed are the related standard deviations, $\sigma_s \eta$, the standard deviations from the mean, $\sigma_s \bar{\eta}$, and the standard deviations from the standard deviation from the mean, $\sigma_s \bar{\mu}$. It is worth remembering that $\log \xi_{\text{vir}} = -x_C$, according to Eq. (39).

η	η_{ADP}	$\bar{\eta}$	$\sigma_s \eta$	$\sigma_s \bar{\eta}$	$\sigma_s \bar{\mu}$
α	0.56832	0.62515	0.13353	0.032860	0.0055541
β	3.3143	3.1132	0.35867	0.086990	0.014919
γ	1.0000	1.0018	0.13893	0.033696	0.0057788
ξ_{vir}	3.6308	6.0210	3.1377	0.76101	0.13051
ν_{mas}	0.55823	1.7340	1.6790	0.40721	0.069837
$\log \xi_{\text{vir}}$	0.56	0.74172	0.17256	0.041852	0.0071775
$\log \nu_{mas}$	-0.25319	0.10544	0.33340	0.080860	0.013867
y_C	4.4	4.5864	0.27926	0.067732	0.011616
b	1.85	1.8480	0.075648	0.018347	0.0031465
b_β	2.544	2.3221	0.21914	0.053149	0.0091151
b_γ	3.84	3.8506	0.21627	0.052454	0.0089958

Table 5: Comparison between parameters, η_{ADP} , related to the best fitting GPL density profile to the mean SDH density profile, and their counterparts, $\bar{\eta}$, averaged over the best fitting GPL density profiles to the whole halo sample, with regard to the minimization of the sum of squares of absolute logarithmic residuals. Also listed are the related standard deviations, $\sigma_s \eta$, the standard deviations from the mean, $\sigma_s \bar{\eta}$, and the standard deviations from the standard deviation from the mean, $\sigma_s \bar{\mu}$. It is worth remembering that $\log \xi_{\text{vir}} = -x_C$, according to Eq. (39).

terparts averaged over the best fitting GPL density profiles to the whole halo sample, as expected from the theory of errors.

- (v) The exponents of best fitting, GPL density profiles, are close to their NFW counterparts, conform to $[\text{Nint}(\alpha), \text{Nint}(\beta), \text{Nint}(\gamma)] = (1, 3, 1)$, where Nint denotes the nearest integer. The difference increases from about one hundredth for γ to about one tenth for β , and to about one half for α .
- (vi) The rms error of the logarithm of the scaled radius, ξ_{vir} , is $\sigma_{s \log \xi_{\text{vir}}} = 0.15 - 0.17$, to be compared with $\sigma_{s \log \xi_{\text{vir}}} = 0.18$ deduced from richer samples where $(\alpha, \beta, \gamma) = (1, 3, 1)$; $M_{\text{vir}} = (0.5-1.0) \times 10^n h^{-1} \text{m}_{\odot}$; $11 \leq n \leq 14$; and n is an integer (Bullock et al. 2001).

6.4 Discussion

The application of a RFSM5 method succeeds in minimizing the sum of absolute values and squares of absolute logarithmic residuals, with respect to GPL density profiles where the exponents are kept fixed, such as NFW, MOA, and RTM, which allows the following definition.

Universal density profile. *Let a RFSM5 method be applied to an assigned set of SDH density profiles. The best fitting GPL density profile to the mean SDH density profile, is defined as the related universal density profile.*

In this view, “universal” has to be intended as nothing but “best fitting”. Strictly speaking, the above statement should apply to a simulated halo sample which is representative of the whole set of real dark matter haloes.

The minimization of the sum of absolute values or squares of absolute logarithmic residuals, makes a firm criterion for deciding which, among two or more GPL density profiles, best fits an assigned SDH density profile. The results of the current paper confirm earlier results about sample haloes on the scale of cluster of galaxies, namely (a) MOA density profiles provide a better fit with respect to NFW (Fukushige & Makino 2001, 2003), and (b) RTM density profiles provide a better fit with respect to NFW (RTM), with the additional result (c) RTM density profiles provide a better fit with respect to MOA.

A RFSM5 method has recently been used for determining the scaled radius (Hiotelis 2003), but using a different definition with respect to $\xi_{\text{vir}} = r_{\text{vir}}/r_0$, Eq. (19). In fact, the usual definition of concentration is $c = r_{\text{vir}}/r_{-2}$, where r_{-2} is the radius related to a logarithmic slope, defined by Eq. (49), $dy/dx = -2$ (e.g., Klypin et al. 2001; Bullock et al. 2001; Hiotelis 2003). The former definition seems to be more general, as it allows the maximum change in slope at the scaled radius, as pointed out in section 2. In addition, it makes the definition of concentration meaningful also in early times, where the slope of a GPL density profile may be smaller (in absolute value) than 2 (Hiotelis 2003).

In dealing with dark matter haloes on the scale of cluster of galaxies, Hiotelis (2003) finds GPL density profiles where the exponent, γ , attains a value of about 1.5, in contrast with the results of the current paper, $\gamma \approx 1$. Such a discrepancy is probably owing to the different definitions of concentration, mentioned above, which have been used.

On the other hand, values of asymptotic inner slopes of fitting density profiles determined in the current paper, are consistent with their counterparts deduced from recent high-resolution simulations using a three-parameter fit involving scaling radius, scaling density, and asymptotic inner slope (6 sample objects, Diemand et al. 2004) or a two-parameter fit involving scaling radius and asymptotic inner slope (16 sample objects, Reed et al. 2005). The related parameters are listed in Tab. 6, which shows agreement between different approaches, within the fiducial range, $\bar{\gamma} \pm 3\sigma_s \bar{\gamma}$. All sample haloes are on the scale of cluster of galaxies, with the exception of three objects belonging to the Reed et al. (2005) sample, which represent SDHs embedding the Milky Way and two dwarf galaxies, respectively. To get a homogeneous sample, a reduced set has been considered, which includes SDHs embedding only clusters of galaxies. A marginal discrepancy between results from the current paper and the original Reed et al. (2005) sample is found to disappear in dealing with the reduced sample, as shown in Tab. 6.

With regard to the asymptotic inner slope of the logarithmic density profile, the current results conform to the validity of the Jeans equation, which demands $1 \leq \gamma \leq 3$ for dark matter haloes (Hansen 2004), but shallower slopes may occur if the effects of the baryonic component are considered (e.g., El-Zant et al. 2004; Hansen 2004). In addition, the inequality, $\gamma < 2$, related to simple analytical treatments of dark matter haloes (Williams et al. 2004), is also fulfilled by the current results, see Tabs. 2-5. On the contrary,

c	n	$\bar{\gamma}$	$\sigma_s \gamma$	$\sigma_s \bar{\gamma}$	$\Delta^- \gamma$	$\Delta^+ \gamma$	$\Delta^\mp \gamma$	$\bar{\gamma}^-$	$\bar{\gamma}^+$
A	17	0.99973	0.16188	0.039261	0.38584	0.25657	0.32120	0.88195	1.1175
S	17	1.0018	0.13893	0.033696	0.29868	0.19820	0.24844	0.90071	1.1029
D	6	1.1617	0.13732	0.056060	0.24167	0.25833	0.25000	0.99352	1.3299
R	16	1.2875	0.23910	0.059774	0.28750	0.41250	0.35000	1.1082	1.4668
R	13	1.2692	0.24285	0.067353	0.26923	0.43077	0.35000	1.0671	1.4713

Table 6: Comparison between statistical parameters related to the asymptotic inner slope, γ , deduced from different samples using different fits. Column captions: 1 - case: A - current paper, minimization of the sum of absolute values of absolute logarithmic residuals; S - current paper, minimization of the sum of squares of absolute logarithmic residuals; D - Diemand et al. (2004); R - Reed et al. (2005); 2 - n : total number of sample objects; 3 - $\bar{\gamma}$: arithmetic mean; 4 - $\sigma_s \gamma$: standard deviation; 5 - $\sigma_s \bar{\gamma}$: standard deviation from the mean; 6 - $\Delta^- \gamma$: maximum negative deviation from the mean; 7 - $\Delta^+ \gamma$: maximum positive deviation from the mean; 8 - $\Delta^\mp \gamma$: mean maximum deviation from the mean; 9 - $\bar{\gamma}^- = \bar{\gamma} - 3\sigma_s \bar{\gamma}$: lower limit assigned to the mean; 10 - $\bar{\gamma}^+ = \bar{\gamma} + 3\sigma_s \bar{\gamma}$: upper limit assigned to the mean. Sample haloes represent clusters or groups, with the exception of three objects belonging to the original R sample (excluded in the reduced R sample), which represent SDHs embedding the Milky Way and two dwarf galaxies, respectively.

the inequality, $\gamma < 1$, related to force-free halo centre and vanishing density at infinite distance (Mücket & Hoefft 2003), is only marginally consistent with the current results.

No evident correlation is found between SDH dynamical state (relaxed or merging) and asymptotic inner slope of the logarithmic density profile, $-\gamma$, or (for SDH comparable virial masses) scaled radius, ξ_{vir} , contrary to previous results (Ascasibar et al. 2004) related to a sample of 19 high-resolution SDHs on the scale of both clusters of galaxies (13 objects) and galaxies (6 objects), with regard to NFW density profiles. An investigation on richer samples could provide more information to this respect.

The GPL density profiles which best fit to the averaged SDH density profile, are characterized by exponents, (α, β, γ) , satisfying $[\text{Nint}(\alpha), \text{Nint}(\beta), \text{Nint}(\gamma)] = (1, 3, 1)$, the last related to NFW density profile. But the corresponding deviations are not negligible with the exception of the one from γ . The comparison with values averaged on the whole halo sample, discloses that the exponents, β and γ , seem to fluctuate around their NFW counterparts, but the same does not hold for α , which has a mean value of about 0.6. Accordingly, NFW density profiles cannot be conceived as universal, in the sense mentioned above, with regard to the current halo sample.

On the other hand, following e.g., Bullock et al. (2001), NFW density profiles (or alternative functional forms) may be considered as a convenient way to parametrize SDH density profiles, without implying that it necessarily provides the best possible fit. This is why the scaled radius, ξ_{vir} , and the scaled mass, ν_{mas} , can be interpreted as general structure parameters, not necessarily restricted to a specific density profile. In particular, any spread in ξ_{vir} and ν_{mas} can be attributed to a real scatter in a “physical” scaling radius, defined by e.g., Eq.(11), rather than to inaccuracies in the assumed, “universal” density profile. For further details see e.g., Bullock et al. (2001).

Additional support to the above considerations is provided by the value calculated for the standard deviation of the decimal logarithm of the scaled radius, $\sigma_{s \log \xi_{\text{vir}}} = 0.15\text{-}0.17$, which is very close to $\sigma_{s \log \xi_{\text{vir}}} = 0.18$ deduced from a statistical sample of about five thousands of simulated haloes, within mass bins equal to $(0.5\text{-}1.0) \times 10^n h^{-1} \text{M}_{\odot}$, where $11 \leq n \leq 14$ and n is an integer (Bullock et al. 2001).

The standard deviations listed in Tabs. 2 and 3, related to characteristic parameters of best fitting GPL density profiles, with regard to sample haloes, have been calculated under the assumption that they obey a Gaussian dis-

tribution, using Eqs. (29)-(32). The existence of a Gaussian distribution is a necessary, but not sufficient condition, for the validity of the central limit theorem. In this view, the parameters under discussion are related to the final properties of the corresponding sample halo, which are connected with the initial conditions, $\alpha_1, \alpha_2, \dots, \alpha_n$, intended as random variables, by a transformation, $\eta^* = \alpha_1 \cdot \alpha_2 \cdot \dots \cdot \alpha_n$. For further details, see Caimmi & Marmo (2004).

In addition, it is worth of note that the application of a least-absolute values or a least-squares method (in particular RFSM5), in fitting GPL to SDH density profiles (e.g., Dubinski & Carlberg 1991; Klypin et al. 2001; Fukushige & Makino 2003) implies a (fiducial) Gaussian distribution of the SDH density profile, $y_{SDH} = \log(\rho_{SDH}/\rho_h)$, around the expected value deduced from the related GPL density profile, $y_{GPL} = \log(\rho_{GPL}/\rho_h)$, for any fixed logarithmic radial bin centered on $x = \log[(r_{i+1} + r_i)/(2r_{\text{vir}})]$. It is the particularization, to the case of interest, of a well known result of the theory of errors (e.g., Taylor 2000, Chap. 8, § 8.2).

The results of the current paper confirm a certain degree of degeneracy in fitting GPL to SDH density profiles, as pointed out by Klypin et al. (2001). For instance, four GPL density profiles fit to the sample halo S02.10, where the sum of absolute values and squares of absolute logarithmic residuals, $\sum |R_i|$ and $\sum R_i^2$, the exponents, α , β , and γ , the scaled radius, ξ_{vir} , the scaled mass, ν_{mas} , the scaling radius, r_0 , and the scaling density, ρ_0 , lie within the following ranges:

$$0.675 < \sum |R_i| < 0.732 \quad ; \quad (33a)$$

$$0.0509 < \sum R_i^2 < 0.0537 \quad ; \quad (33b)$$

$$0.559 < \alpha < 0.727 \quad ; \quad (33c)$$

$$2.73 < \beta < 3.37 \quad ; \quad (33d)$$

$$0.818 < \gamma < 0.943 \quad ; \quad (33e)$$

$$3.89 < \xi_{\text{vir}} < 8.04 \quad ; \quad (33f)$$

$$0.431 < \nu_{\text{mas}} < 3.10 \quad ; \quad (33g)$$

$$409 < r_0/\text{kpc} < 847 \quad ; \quad (33h)$$

$$1.28 < 10^4 \rho_0 / (10^{10} \text{M}_\odot / \text{kpc}^3) < 1.70 \quad ; \quad (33i)$$

which could be explained in a twofold manner.

On one hand, a degeneracy could be intrinsic to the 6-dimension hyperspace where the RFSM5 method works. Accordingly, the 5-dimension hypersurface, $w = F(x_C, y_C, b, b_\beta, b_\gamma)$, defined by the sum of absolute values or squares of absolute logarithmic residuals, happens to be parallel, in some finite region of the domain, to the principal 5-dimension hyperplane, $(O \ x_C \ y_C \ b \ b_\beta \ b_\gamma)$, which implies infinite extremum points of minimum⁵.

On the other hand, a degeneracy could be owing to the restricted domain of SDH density profiles, defined by Eq. (17), which is limited by the virial radius on the right and by the occurrence of numerical artifacts (mainly two-body relaxation) on the left. In this view, a more extended range could reduce the degeneracy. As the fit must necessarily be restricted to the virialized region, one shall wait for higher-resolution simulations involving five-parameter fits to test this possibility. But in recent high-resolution simulations two or three-parameter fits only have been used (e.g., Navarro et al. 2004; Diemand et al. 2004; Reed et al. 2005).

The current attempt is limited to GPL density profiles, defined by Eq. (1), but different alternatives have been exploited in the literature, such as the Burkert (1995) density profile:

$$\rho = \rho_0 \left[1 + \left(\frac{r}{r_0} \right)^2 \right]^{-1} \left[1 + \frac{r}{r_0} \right]^{-1} ; \quad (34)$$

which resembles the NFW density profile for $r \gtrsim 0.02r_{\text{vir}}$. The corresponding scaling and scaled radii may be related as: $(r_0)_B = (r_0)_{\text{NFW}}/1.52$; $(\xi_{\text{vir}})_B = 1.52(\xi_{\text{vir}})_{\text{NFW}}$; respectively (e.g., Bullock et al. 2001).

Another possibility is a profile that curves smoothly over to a constant density at very small radii (Navarro et al. 2004):

$$\rho = \rho_0 \exp \left\{ -\frac{2}{\lambda} \left[\left(\frac{r}{r_0} \right)^\lambda - 1 \right] \right\} ; \quad (35)$$

where the parameter, λ , prescribes how fast the density profile turns away from a power-law near the centre. In logarithmic form, Eq.(35) represents

⁵An example in a 3-dimension space, $(Oxyz)$, is provided by the surface of a cylinder: in the special case where the height, or a basis, is parallel to the principal plane, (Oxy) , infinite extremum points of minimum occur. If otherwise, there is a single extremum point of minimum.

a class (defined by the parameter, $-2/\lambda$) of Sersic (1968) density profiles (Merritt et al. 2005). The best fit reads (19 sample objects, Navarro et al. 2004): $\bar{\lambda} \mp 3\sigma_s \bar{\lambda} = 0.17216 \mp 0.021897$.

On the other hand, the RFSM5 method may be extended to any kind of density profile, keeping in mind that different classes could exhibit different geometrical properties.

The “universality” of density profiles involving scaled parameters, has to be intended as in polytropes (e.g., Caimmi 1980).

A single distribution in the abstract space of the scaled variables, $\phi = f(\xi)$, corresponds to ∞^2 distributions in the physical space, $\rho/\rho_0 = f(r/r_0)$, provided the free parameters are the scaling radius, r_0 , and the scaling density, ρ_0 , and the scaled radius reads $\xi = r/r_0$.

In dealing with SDH density profiles, it would be more germane to the matter speaking about best fitting, instead of universal, density profiles. The validity of the fit has to be restricted to a fiducial range where simulations are not affected by spurious effects such as two-body relaxation, according to e.g., Eq. (17). In particular, the asymptotic inner slope is necessary for the definition of GPL density profiles, but any conclusion outside the above mentioned fiducial range may be at risk, in absence of some kind of (direct or indirect) observational support.

7 Conclusion

Analytical and geometrical properties of generalized power-law (GPL) density profiles have been investigated in detail. In particular, a one-to-one correspondence has been found between mathematical parameters (a scaling radius, r_0 , a scaling density, ρ_0 , and three exponents, α , β , γ), and geometrical parameters (the coordinates of the intersection of the asymptotes, x_C , y_C , and three vertical intercepts, b , b_β , b_γ , related to the curve and the asymptotes, respectively): $(r_0, \rho_0, \alpha, \beta, \gamma) \leftrightarrow (x_C, y_C, b, b_\beta, b_\gamma)$.

Then GPL density profiles have been compared with simulated dark haloes (SDH) density profiles, and nonlinear least-absolute values and least-squares fits involving the above mentioned five parameters (RFSM5 method) have been prescribed. More specifically, the sum of absolute values or squares of absolute logarithmic residuals, $R_i = \log \rho_{SPH}(r_i) - \log \rho_{GPL}(r_i)$, has been

evaluated on 10^5 points making a 5-dimension hypergrid, through a few iterations. The size has progressively been reduced around a fiducial minimum, and superpositions on nodes of earlier hypergrids have been avoided.

An application has been made to a sample of 17 SDHs on the scale of cluster of galaxies, within a flat Λ CDM cosmological model (Rasia et al. 2004). In dealing with the mean SDH density profile, a virial radius, r_{vir} , averaged over the whole sample, has been assigned, which has allowed the calculation of the remaining parameters. Using a RFSM5 method has provided a better fit with respect to other methods.

The geometrical parameters, averaged over the whole sample of best fitting GPL density profiles, have yielded $(\alpha, \beta, \gamma) \approx (0.6, 3.1, 1.0)$, to be compared with $(\alpha, \beta, \gamma) = (1, 3, 1)$, i.e. the NFW density profile (Navarro et al. 1995, 1996, 1997); $(\alpha, \beta, \gamma) = (1.5, 3, 1.5)$ (Moore et al. 1998, 1999); $(\alpha, \beta, \gamma) = (1, 2.5, 1)$ (Rasia et al. 2004); and, in addition, $\gamma \approx 1.5$ (Hiotelis 2003), deduced from the application of a RFSM5 method, but using a different definition of scaled radius, or concentration; $\gamma \approx 1.2$ -1.3 deduced from more recent fits (Diemand et al. 2004; Reed et al. 2005). No evident correlation has been found between SDH dynamical state (relaxed or merging) and asymptotic inner slope of the logarithmic density profile or (for SDH comparable virial masses) scaled radius.

Mean values and standard deviations of some parameters have been calculated, and in particular the decimal logarithm of the scaled radius, ξ_{vir} , has been found to yield $\langle \log \xi_{\text{vir}} \rangle = 0.74$ and $\sigma_{s \log \xi_{\text{vir}}} = 0.15$ -0.17, consistent with previous results related to NFW density profiles. It has provided additional support to the idea, that NFW density profiles may be considered as a convenient way to parametrize SDH density profiles, without implying that it necessarily produces the best possible fit (Bullock et al. 2001).

A certain degree of degeneracy has been found in fitting GPL to SDH density profiles. If it is intrinsic to the RFSM5 method or it could be reduced by the next generation of high-resolution simulations, still remains an open question.

Future work demands a generalization of the above results on two respects. First, the method could be applied to data related to dynamical mass distributions inferred in cluster of galaxies (or galaxies), and the fit be compared with its counterpart deduced from simulated density profiles. Second, the method could be applied using Sersic (1968) density profiles in place of the family defined by Eq. (1). An advantage is that both baryonic

and dark (non baryonic) mass distributions are well represented by the Sersic law (Merritt et al. 2005), which depends on four parameters instead of five.

8 Acknowledgements

We are indebted with E. Rasia, G. Tormen, and L. Moscardini, for making the results of their simulations, investigated in RTM, available to us. In addition, we are deeply grateful to all of them for clarifying and fruitful discussions. We thank two anonymous referees for useful critical comments.

References

- [1] Ascasibar, Y., Yepes, G., Gottlöber, S., & Müller, V. 2003, MRNAS, 352, 1109
- [2] Arieli, Y., & Rephaeli, Y. 2003, NewA, 8, 517
- [3] Binney, J., & Evans, N.W. 2001, MNRAS, 327, L27
- [4] Bullock, J. S., Kolatt, T. S., Sigad, Y., et al. 2001, MNRAS, 321, 559
- [5] Burkert, A. 1995, ApJ, 447, L25
- [6] Caimmi, R. 1980 ApSS, 71, 415
- [7] Caimmi, R., & Marmo, C. 2003, NewA, 8, 119
- [8] Caimmi, R., & Marmo, C. 2004, SAJ 169, 11
- [9] Cole, S., & Lacey, C. 1996, MNRAS, 281, 716
- [10] de Blok, W.J.G., McGaugh, S.S., & Rubin, V.C. 2001, AJ, 122, 2396
- [11] Dehnen, W. 1993, MNRAS 265, 250
- [12] Diemand, J., Moore, B., Stadel, J. 2004, MNRAS, 353, 624
- [13] El-Zant, A.A., Hoffman, J., Primack, J., Combes, F., & Sloshman, I. 2004, ApJ, 607, L75

- [14] Dubinski, J., & Carlberg, R.G. 1991, ApJ, 378, 496
- [15] Fukugita, M., Peebles, P.J.E. 2004, ApJ 616, 643
- [16] Fukushige, T., & Makino, J. 1997, ApJ, 477, L9
- [17] Fukushige, T., & Makino, J. 2001, ApJ, 557, 533
- [18] Fukushige, T., & Makino, J. 2003, ApJ, 588, 674
- [19] Fukushige, T., Kawai, A., & Makino, J., 2004, ApJ, 606, 625
- [20] Ghigna, S., Moore, B., Governato, F., Lake, G., Quinn, T., & Stadel, J. 2000, ApJ, 544, 616
- [21] Hansen, S.H. 2004, MNRAS, 352, L41
- [22] Hernquist, L. 1990, ApJ, 356, 359
- [23] Hiotelis, N. 2003, MNRAS, 344, 149
- [24] Huss, A., Jain, B., & Steinmetz, M. 1999, ApJ, 517, 64
- [25] Jing, Y.P., & Suto, Y. 2000, ApJ, 529, L69
- [26] Klypin, A., Kravtsov, A.V., Bullok, J.S., & Primack, J.R. 2001, ApJ, 554, 903
- [27] Kuzmin, G.G., Veltmann, U.K. 1973, Publ. Tart. Astrof. Obs. im. V. Struve, 40, 281
- [28] McGaugh, S.S., & de Blok, W.J.G. 1988, ApJ, 499, 66
- [29] Merritt, D., Navarro, J.F., Ludlow, A., Jenkins, A., 2005, ApJ 624, L85
- [30] Moore, B., Governato, F., Quinn, T., Stadel, J., & Lake, G. 1998, ApJ, 499, L5
- [31] Moore, B., Quinn, T., Governato, F., Stadel, J., & Lake, G. 1999 MNRAS, 310, 1147
- [32] Mückel, J.P., & Hoefft, M. 2003, A&A, 404, 809

- [33] Navarro, J.F., Frenk, C.S., & White, S.D.M. 1995, MNRAS, 275, 720
- [34] Navarro, J.F., Frenk, C.S., & White, S.D.M. 1996, ApJ, 462, 563
- [35] Navarro, J.F., Frenk, C.S., & White, S.D.M. 1997, ApJ, 490, 493 (NFW)
- [36] Navarro, J.F., Hayashi, E., Power, C., et al., 2004, MNRAS, 349, 1039
- [37] Oliva, P.R., & Terrasi, F. 1976, *Elaborazione statistica dei risultati sperimentali*, Liguori Editore, Napoli
- [38] Padoan, P., Nordlund, A., & Jones, B.J.R. 1997, MNRAS, 288, 145
- [39] Rasia, E., Tormen, G., & Moscardini, L. 2004, MNRAS, 351, 237 (RTM)
- [40] Reed, D., Governato, F., Verde, L., et al. 2005, MNRAS, 357, 82
- [41] Ricotti, M. 2003, MNRAS, 344, 1237
- [42] Rubiño-Martin, J.A., Rebolo, R., Carreira, P., et al. 2003, MNRAS, 341, 1084
- [43] Secco, L. 2001, *Gli errori nelle misure fisiche*, CUSL Nuova Vita, Padova
- [44] Sersic, J.L. 1968, Atlas de Galaxies Australes Cordoba: Obs. Astron., Univ. Nac. Cordoba
- [45] Sievers, J.L., Bond, J.R., Cartwright, J.K., et al. 2003, ApJ, 591, 599
- [46] Syer, D., & White, S. D. M. 1998, MNRAS, 293, 337
- [47] Spergel, D.N., Verde, L., Peiris, H.V., et al. 2003, ApJSupp, 148, 175
- [48] Tasitsiomi, A., Kravstov, A.V., Gottlöber, S., Klypin, A.A. 2004, ApJ, 607, 125
- [49] Taylor, J.R. 2000, *Introduzione all'analisi degli errori*, Zanichelli, Bologna
- [50] Tremaine, S., Richstone, D.O., Byun, Y., et al. 1994, AJ 107, 634
- [51] van den Bosh, F.C., & Swaters, R.A. 2001, MNRAS, 325, 1017

- [52] Williams, L.L.R., Babul, A., & Dalcanton, J.J, 2004. ApJ, 604, 18
- [53] Zhao, H.S. 1996, MNRAS, 278, 488
- [54] Zhao, H.S. 1997, MNRAS, 287, 525
- [55] Zhao, D.H., Mo, H.J., Jing, J.P., & Börner, G. 2003, MNRAS, 339, 12

9 Appendix

9.1 A. Analytical and geometrical properties of logarithmic GPL density profiles

The values of the vertical intercept related to the curve, b , and to the asymptotes, b_β and b_γ , are readily determined by putting $\log \eta = 0$ i.e. $\eta = 1$ in Eqs. (22), (25), and (26), respectively. The result is:

$$b = \log \Delta_{\text{vir}} - \log \nu_{\text{mas}} + 3 \log \xi_{\text{vir}} - \gamma \log \xi_{\text{vir}} - \chi \log(1 + \xi_{\text{vir}}^\alpha) ; \quad (36)$$

$$b_\gamma = \log \Delta_{\text{vir}} - \log \nu_{\text{mas}} + 3 \log \xi_{\text{vir}} - \gamma \log \xi_{\text{vir}} ; \quad (37)$$

$$b_\beta = \log \Delta_{\text{vir}} - \log \nu_{\text{mas}} + 3 \log \xi_{\text{vir}} - \beta \log \xi_{\text{vir}} ; \quad (38)$$

for sake of brevity, let us denote the intersection of the asymptotes in the logarithmic plane, $(\text{O } \log \eta \log \psi)$, as $\mathcal{C}(x_C, y_C)$ where, owing to Eqs. (18), (19), (25), (26), (37), and (38), the explicit expression of the coordinates reads:

$$x_C = -\log \xi_{\text{vir}} = -\log \frac{r_{\text{vir}}}{r_0} = \log \frac{r_0}{r_{\text{vir}}} ; \quad (39)$$

$$y_C = \log \frac{\Delta_{\text{vir}} \xi_{\text{vir}}^3}{\nu_{\text{mas}}} = \log \frac{\rho_0}{\rho_h} ; \quad (40)$$

which yields the following.

Theorem. *For a selected (but arbitrary) SDH density profile, cosmological model, and GPL density profile, the intersection of the asymptotes in the logarithmic plane, $(\text{O } \log \eta \log \psi)$, occurs at a point, $\mathcal{C}(x_C, y_C)$, where the coordinates are the decimal logarithm of the ratio between scaling radius and virial radius, and scaling density and mean (matter) density of the universe, respectively.*

The combination of Eqs. (18), (19), (39), and (40) yields:

$$\log \nu_{mas} = \log \Delta_{\text{vir}} - 3x_C - y_C ; \quad (41)$$

accordingly, the vertical intercepts of the curve and the asymptotes, expressed by Eqs. (36), (37), and (38), reduce to:

$$b = y_C + \gamma x_C - \chi \log [1 + \exp_{10}(-\alpha x_C)] ; \quad (42)$$

$$b_\gamma = y_C + \gamma x_C ; \quad (43)$$

$$b_\beta = y_C + \beta x_C ; \quad (44)$$

where, in general, $\exp_u x = u^x$, and $\exp x = e^x$, according to the standard notation.

A change of coordinates, defined as:

$$x = \log \eta ; \quad y = \log \psi ; \quad (45)$$

makes the expressions of the curve and the asymptotes, defined by Eqs. (22), (25), and (26), translate into:

$$y = y_C - \gamma(x - x_C) - \chi \log\{1 + \exp_{10}[\alpha(x - x_C)]\} ; \quad (46)$$

$$y = y_C - \gamma(x - x_C) ; \quad x \ll x_C ; \quad (47)$$

$$y = y_C - \beta(x - x_C) ; \quad x \gg x_C ; \quad (48)$$

with regard to the plane (Oxy).

The first derivative of the curve, defined by Eq. (46), takes the expression:

$$\frac{dy}{dx} = -\beta + \frac{\beta - \gamma}{1 + \exp_{10}[\alpha(x - x_C)]} ; \quad (49)$$

and the particularization of the above result to the vertical intercept of the curve, reads:

$$\left(\frac{dy}{dx} \right)_{x=0} = -\beta + \frac{\beta - \gamma}{1 + \exp_{10}(-\alpha x_C)} ; \quad (50)$$

according to Eqs. (42) and (50), the equation of the tangent to the curve at the vertical intercept is:

$$y = \left[-\beta + \frac{\beta - \gamma}{1 + \exp_{10}(-\alpha x_C)} \right] x + b ; \quad (51)$$

the intersections of this line with the asymptotes, expressed by Eqs. (47) and (48), let them be $\mathbf{M}(x_M, y_M)$ and $\mathbf{R}(x_R, y_R)$, respectively, may be calculated after some algebra. The result is:

$$x_M = \frac{b_\beta - b}{\beta - \gamma} [1 + \exp_{10}(-\alpha x_C)] \quad ; \quad (52)$$

$$y_M = b_\beta - \beta \frac{b_\beta - b}{\beta - \gamma} [1 + \exp_{10}(-\alpha x_C)] \quad ; \quad (53)$$

$$x_R = -\frac{b_\gamma - b}{\beta - \gamma} [1 + \exp_{10}(-\alpha x_C)] \quad ; \quad (54)$$

$$y_R = b_\gamma + \gamma \frac{b_\gamma - b}{\beta - \gamma} [1 + \exp_{10}(-\alpha x_C)] \quad ; \quad (55)$$

the curve, the tangent to the curve at the vertical intercept, and the asymptotes, are represented in Fig. 6. It is apparent that the curve must necessarily lie below the asymptotes and the segment, $\overline{\mathbf{MR}}$, with the exception of the tangential point, $\mathbf{B}(0, b)$.

The combination of Eqs. (42), (43), and (44) yields:

$$b_\gamma - b = \chi \log [1 + \exp_{10}(-\alpha x_C)] \quad ; \quad (56)$$

$$b_\beta - b_\gamma = (\beta - \gamma)x_C = \chi \alpha x_C \quad ; \quad (57)$$

and the comparison between the alternative expressions of the exponent, χ , deduced from Eqs. (56), (57), produces:

$$Aw = \log [1 + \exp_{10} w] \quad (58a)$$

$$A = \frac{b_\gamma - b}{b_\gamma - b_\beta} > 1 \quad ; \quad (58b)$$

$$w = -\alpha x_C > 0 \quad ; \quad (58c)$$

which is equivalent to:

$$u^A - u - 1 = 0 \quad ; \quad (59a)$$

$$u = \exp_{10} w \quad ; \quad (59b)$$

where $A > 1$, $w > 0$, and $-\beta < -\gamma < 0$, in the case of interest (logarithmic GPL density profiles of the kind represented in Fig. 6).

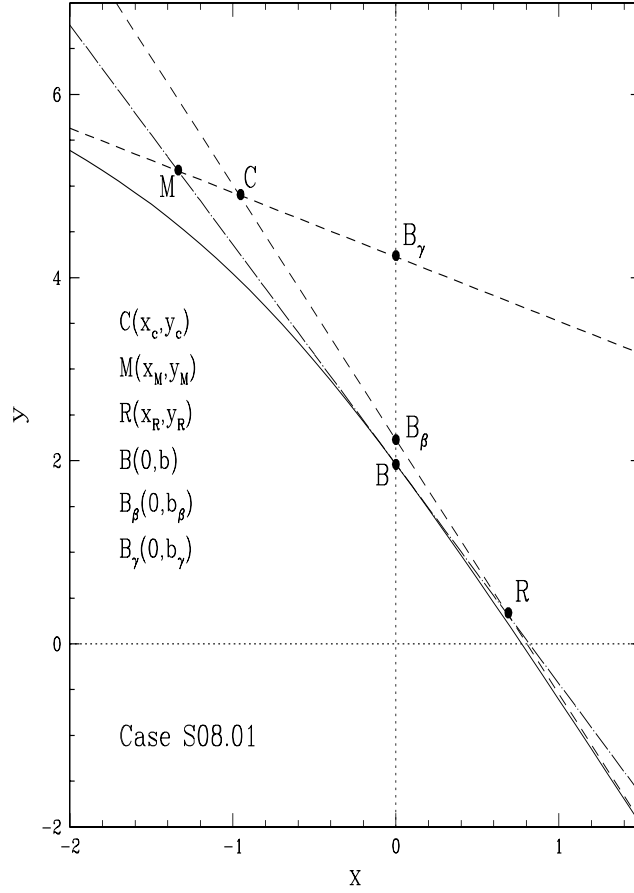


Figure 6: A NFW logarithmic density profile, together with the tangent at the vertical intercept and the asymptotes, on the (Oxy) plane. The above mentioned straight lines define a triangle, CMR . The curve must necessarily lie below the asymptotes and the segment, \overline{MR} , with the exception of the tangential point, B .

The function, $\phi(u)$, on the left-hand side of Eq. (59a), has the following properties:

$$\phi(u) = u^A - u - 1 \quad ; \quad 0 \leq u < +\infty \quad ; \quad (60a)$$

$$\phi(0) = -1 \quad ; \quad u_{min} = A^{-1/(A-1)} \quad ; \quad (60b)$$

$$\lim_{u \rightarrow +\infty} \phi(u) = +\infty \quad \phi(u_0) = 0 \quad ; \quad (60c)$$

where u_{min} and u_0 denote the abscissa of the extremum point (of minimum) and the zero of the function, respectively. Then Eq. (59a) may be solved by use of an iterative method.

The combination of Eqs. (57), (58c), and (59b) yields:

$$\alpha = -\frac{\log u_0}{x_C} \quad ; \quad (61)$$

$$\chi = \frac{b_\gamma - b_\beta}{\log u_0} \quad ; \quad (62)$$

on the other hand, the exponents, γ and β , may be deduced from Eqs. (43) and (44), respectively, as:

$$\gamma = \frac{b_\gamma - y_C}{x_C} \quad ; \quad (63)$$

$$\beta = \frac{b_\beta - y_C}{x_C} \quad ; \quad (64)$$

and the scaling parameters, r_0 and ρ_0 , may be deduced from Eqs. (39) and (40), respectively, as:

$$r_0 = r_{vir} \exp_{10} x_C \quad ; \quad (65)$$

$$\rho_0 = \rho_h \exp_{10} y_C \quad ; \quad (66)$$

the set of Eqs. (61)-(66) yields the following.

Theorem. *For a selected (but arbitrary) SPH density profile, cosmological model, and GPL density profile, in the logarithmic plane, (Oxy) , there is a one-to-one correspondence between analytical parameters, $(r_0, \rho_0, \alpha, \beta, \gamma)$, and geometrical parameters, $(x_C, y_C, b, b_\beta, b_\gamma)$, in the sense that either set univocally determines a GPL density profile.*

The advantage of using geometrical instead of analytical parameters lies in a better understanding of how the curve change as one or more parameters do.

With regard to SDH density profiles, according to Eqs. (17) and (45), let us divide the domain into two distinct regions, as:

$$-2 \leq x_\gamma \leq -1 \quad ; \quad -1 \leq x_\beta \leq 0 \quad ; \quad (67)$$

which shall be called the γ region and the β region, respectively.

Let (x_i, y_i) be coordinates of a generic point of a logarithmic SDH density profile, and $[x_i, y(x_i)]$ their counterparts related to a fitting, logarithmic GPL density profile. Owing to Eq. (46), the corresponding, logarithmic absolute residual, is:

$$R_i = y_i - y(x_i) = y_i - y_C + \gamma(x_i - x_C) + \chi \log\{1 + \exp_{10}[\alpha(x_i - x_C)]\} \quad ; \quad (68)$$

the particularization of Eq. (68) to the γ and β region, defined by Eq. (67), allows the application of a least-squares fit to the related portions of SDH density profile. The best linear fites are:

$$y = b_{s\gamma} - \gamma_s x \quad ; \quad (69)$$

$$y = b_{s\beta} - \beta_s x \quad ; \quad (70)$$

and the coordinates of their intersection point, $C_s(x_s, y_s)$, are:

$$x_s = \frac{b_{s\gamma} - b_{s\beta}}{\beta_s - \gamma_s} \quad ; \quad y_s = \frac{b_{s\gamma}\beta_s - b_{s\beta}\gamma_s}{\beta_s - \gamma_s} \quad ; \quad (71)$$

the best linear fits to a selected SDH density profile, are plotted in Fig. 2.

The intercepts, $b_{s\gamma}$ and $b_{s\beta}$, and the slopes, $-\gamma_s$ and $-\beta_s$, appearing in Eqs. (69) and (70), are calculated using the standard formulation of the method (e.g., Secco 2001, Chap. 4, § 4.1):

$$-\lambda_s = \frac{\overline{x_\lambda y_\lambda} - \overline{x_\lambda} \overline{y_\lambda}}{\overline{x_\lambda x_\lambda} - \overline{x_\lambda} \overline{x_\lambda}} \quad ; \quad (72)$$

$$b_{s\lambda} = \frac{\overline{y_\lambda x_\lambda x_\lambda} - \overline{x_\lambda} \overline{x_\lambda x_\lambda}}{\overline{x_\lambda x_\lambda} - \overline{x_\lambda} \overline{x_\lambda}} \quad ; \quad (73)$$

$$\sigma_s^2_{\lambda_s} = \sigma_s^2_{y_\lambda} \frac{1}{\overline{x_\lambda x_\lambda} - \overline{x_\lambda} \overline{x_\lambda}} \quad ; \quad (74)$$

$$\sigma_s^2_{b_s} = \sigma_s^2_{y_\lambda} \frac{\overline{x_\lambda x_\lambda}}{\overline{x_\lambda x_\lambda} - \overline{x_\lambda} \overline{x_\lambda}} \quad ; \quad (75)$$

where $\lambda = \beta, \gamma$, a bar denotes arithmetic mean over the corresponding range of simulated values, and σ_s^2 is the empirical variance of the histogram calculated for the selected random variable.

The comparison between best linear fits to SDH density profiles, defined by Eqs. (69) and (70), and related asymptotes of GPL density profiles, defined by Eqs. (47) and (48), implies the following, fiducial conclusions: (i) SDH best linear fits lie below related GPL asymptotes, in the range of interest, and (ii) SDH best linear fits are more inclined (in absolute value) with respect to related GPL asymptotes towards negative infinite, and less inclined (in absolute value) with respect to related GPL asymptotes towards positive infinite. Accordingly (iii) the intersection between SDH best linear fits lies below, and on the left, with respect to the intersection of related GPL asymptotes.

The above mentioned conclusions (i) and (ii) read:

$$b < b_{s\beta} \ ; \quad b_{s\beta} < b_\beta \ ; \quad b_{s\gamma} < b_\gamma \ ; \quad (76)$$

$$\gamma_s < \gamma < 0 \ ; \quad \beta < \beta_s < \gamma_s \ ; \quad (77)$$

on the other hand, GPL asymptotes intersect within the $(-+)$ quadrant, according to Eqs. (39) and (40), which yields:

$$b < y_C \ ; \quad b_\beta < y_C \ ; \quad b_\gamma < y_C \ ; \quad (78)$$

finally, lower and upper values to the ranges:

$$y_{min} < y_C < y_{max} \ ; \quad x_{min} < x_C < x_{max} \ ; \quad (79)$$

and the lower value to the range:

$$b_{min} < b < b_{s\beta} \ ; \quad (80)$$

may be deduced from SDH density profiles. The upper value of inequality (80) is owing to the first inequality (76). The combination of inequalities (76) and (78) yields:

$$b_{s\beta} < b_\beta < y_C \ ; \quad b_{s\gamma} < b_\gamma < y_C \ ; \quad (81)$$

due to negative slopes of GPL asymptotes, $-\gamma < 0$ and $-\beta < 0$.

With regard to a 5-dimension hyperspace, $(O \ x_C \ y_C \ b \ b_\beta \ b_\gamma)$, inequalities (79), (80), and (81), define a 5-dimension hyperrectangle of sides $(x_{max} - x_{min})$, $(y_{max} - y_{min})$, $(b_{s\beta} - b_{min})$, $(y_{max} - b_{s\beta})$, and $(y_{max} - b_{s\gamma})$, respectively. Then it is possible to make a 5-dimension hypergrid where the points are equally spaced; according to inequalities (81), the ranges $y_C < b_\beta < y_{max}$ and $y_C < b_\gamma < y_{max}$ are to be excluded as outside the cases of interest. In dealing with the remaining points, the sum of both absolute values and squares of absolute logarithmic residuals, defined by Eq. (68), is performed, and the minimum on the hypergrid is determined in each alternative. Let it be $(x_C^{(a)}, y_C^{(a)}, b^{(a)}, b_\beta^{(a)}, b_\gamma^{(a)})$ and $(x_C^{(s)}, y_C^{(s)}, b^{(s)}, b_\beta^{(s)}, b_\gamma^{(s)})$, where the indices, a and s , denote absolute value and square, respectively.

The next iteration is in connection with a 5-dimension hyperrectangle, which has the following features: (1) it is centered near the previously determined point of minimum; (2) it is reduced in size by a factor of about 10, provided inequalities (79), (80), and (81) continue to hold; and (3) there is no point in common with the earlier hypergrid. Then two additional points of minimum are calculated and the next iteration is allowed to start.

The computations end when the sum of absolute values and squares of absolute logarithmic residuals fall below an assigned treshold, which yields:

$$\sum_{i=1}^N |R_i| < \epsilon^{(a)} \quad ; \quad (82)$$

$$\sum_{i=1}^N R_i^2 < \epsilon^{(s)} \quad ; \quad (83)$$

where the sum is performed on the range of interest, defined by Eq. (67).